The ant and the grasshopper: Contrasting responses and behaviors to water stress of riparian trees along a hydroclimatic gradient

Pierre Lochin, Pauline Malherbe, Baptiste Marteau, Julien Godfroy, Flavie Gerle, John Marshall, Sara Puijalon, Michael Bliss Singer, John C Stella, Hervé Piégay, et al.

Science of the Total Environment 952 (2024) 175916

Contents lists available at ScienceDirect

Science of the Total Environment

journal homepage: www.elsevier.com/locate/scitotenv

The ant and the grasshopper: Contrasting responses and behaviors to water stress of riparian trees along a hydroclimatic gradient

Pierre Lochin [a,*], Pauline Malherbe [a], Baptiste Marteau [a,b], Julien Godfroy [a,c], Flavie Gerle [d], John Marshall [e,f,g], Sara Puijalon [d], Michael Bliss Singer [h,i,j], John C. Stella [k], Hervé Piégay [a], Antoine Vernay [d]

[a] ENS de Lyon, UMR 5600 Environnement Ville société, CNRS, Lyon, France
[b] LETG UMR 6554, Université Rennes 2, Rennes, France
[c] Univ. Grenoble Alpes, INRAE, LESSEM, F-38402 St-Martin d'Hères, France
[d] Université Claude Bernard Lyon 1, LEHNA UMR 5023, CNRS, ENTPE, F-69622, Villeurbanne, France
[e] Global Change Research Institute, Czech Academy of Sciences, Bělidla 4a, 603 00 Brno, Czech Republic
[f] Leibniz-Zentrum für Agrarlandschaftsforschung, 15374 Müncheberg, Germany
[g] Department of Geological Sciences, Gothenburg University, Gothenburg, Sweden
[h] Earth Research Institute, University of California, Santa Barbara, CA 93106, USA
[i] Water Research Institute, Cardiff University, Cardiff CF10 3AX, UK
[j] School of Earth and Environmental Sciences, Cardiff University, Cardiff CF10 3AT, UK
[k] Department of Sustainable Resources Management, State University of New York College of Environmental Science and Forestry, Syracuse, NY 13210, USA

HIGHLIGHTS

- Remote sensing and ecophysiological data can help understand white poplar drought responses at large spatial scales.
- Tree water stress was estimated in different water availability contexts.
- Infrared thermal measurements were associated with water use strategy traits.
- Less drought-prone trees have lower ecophysiological control of water loss.
- Multi-scale and multi-tool analyses are needed for studying water stress responses.

GRAPHICAL ABSTRACT

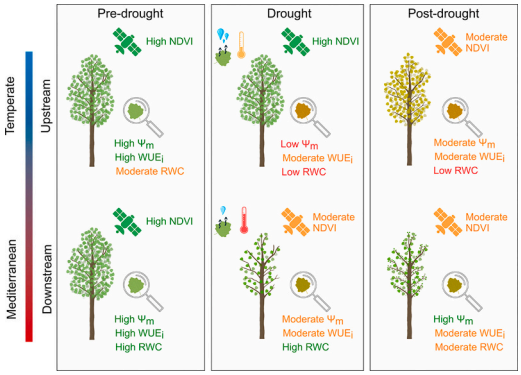

ARTICLE INFO

Editor: Sergi Sabater

Keywords:
Populus alba
White poplar
Remote sensing

ABSTRACT

Riparian trees are particularly vulnerable to drought because they are highly dependent on water availability for their survival. However, the response of riparian tree species to water stress varies depending on regional hydroclimatic conditions, making them unevenly vulnerable to changing drought patterns. Understanding this spatial variability in stress responses requires a comprehensive assessment of water stress across broader spatial and temporal scales. Yet, the precise ecophysiological mechanisms underlying these responses remain poorly

* Corresponding author.
E-mail address: pierre.lochin@ens-lyon.fr (P. Lochin).

https://doi.org/10.1016/j.scitotenv.2024.175916
Received 29 March 2024; Received in revised form 27 August 2024; Accepted 29 August 2024
Available online 1 September 2024

Thermal infrared
Water content
Water potential

linked to remotely sensed indices. To address this gap, the implementation of remote sensing methods coupled with in situ validation is essential to obtain consistent results across diverse spatial and temporal contexts. We conducted a multi-tool analysis combining multispectral and thermal remote sensing indices with in situ ecophysiological measurements at different temporal scales to analyze the responses of white poplar (*Populus alba*) to seasonal changes in drought along a hydroclimatic gradient.

Using this approach, we demonstrate that white poplars along the Rhône River (France) exhibit contrasting responses and behaviors during drought depending on the latitudinal context. White poplars in a Mediterranean climate show rapid stomatal closure to reduce water loss and maintain high minimum water potential levels, although this results in a decrease in remotely sensed greenness. Conversely, white poplars located upstream in a temperate climate show high transpiration and stable greenness but lower minimum water potential and water content. A site in the middle of the gradient has intermediate responses. These results demonstrate that white poplars along a climate gradient can have a range of responses to drought along the iso/anisohydricity continuum.

These results are important for future climatic conditions because they show that the same species can have different mechanisms of drought resilience, even in the same river valley. This raises questions regarding how these riparian tree populations will respond to future climatic and hydrological conditions.

1. Introduction

The increasing frequency and severity of droughts associated with global change is a threat to riparian tree resilience (Choat et al., 2018; Peters et al., 2021; Reichstein et al., 2013), yet the role of riparian ecosystems is fundamental in the adaptation of other ecosystems to global change (Capon et al., 2013; Perry et al., 2012; Zhang et al., 2023). In the face of increasing water stress, tree species may exhibit different strategies to cope with drought through species-specific hydraulic traits (Anderegg et al., 2016; McDowell et al., 2022). These traits may confer greater resilience to drought in some species but may also vary within the same species (Fuchs et al., 2021; Viger et al., 2016), making some trees more resilient to water deficits. However, little is known about these intraspecific differences, and they need to be better understood to anticipate future tree responses to increased water stress, especially in non-drought-prone environments where tree responses remain uncertain. Can trees adapt and withstand drought by behaving like the ant in Aesop's fable, conserving water resources for long-term survival? Or will they continue to function normally, like the grasshopper, but to the detriment of their resilience to drought? To understand the potential responses of trees to future changing drought conditions, it is necessary to analyze the responses of riparian trees in various hydroclimatic contexts and assess water stress signals at broad spatial and temporal scales to gain a better overall understanding of their responses to water stress.

Riparian trees are particularly vulnerable and sensitive to fluctuations in water availability because they rely primarily on soil moisture and groundwater availability for their long-term survival (Friedman et al., 2022; Pettit and Froend, 2018; Sabathier et al., 2021; Sargeant and Singer, 2021; Singer et al., 2014; Warter et al., 2023). A common response of trees to drought is to reduce their stomatal conductance, which prevents excessive canopy transpiration and reduces water loss and the risk of cavitation, but at the cost of slower growth and development. Therefore, prolonged periods of water scarcity and anthropogenic alterations of streamflow and groundwater levels can have detrimental effects on riparian tree growth and health. Drought-related growth decline and mortality have been documented in riparian trees, mostly in semiarid environments (Pettit and Froend, 2018; Rivaes et al., 2013; Stromberg et al., 1996). More recently, studies have expanded the scope of interest by analyzing riparian forest responses to drought at the scale of entire drainage basins (Kibler et al., 2021; Pace et al., 2021; Rohde et al., 2021). However, these studies only examined riparian stand responses using remote sensing, without accounting for specific individuals or considering climatic variability. As a result, our understanding of how riparian forests respond to changing drought conditions remains limited (Portela et al., 2023; Slette et al., 2019), especially across hydroclimatic gradients (Palmer et al., 2008; Williams et al., 2022). Interspecific ecophysiological responses along hydroclimatic gradients have shown that species in the driest zones have higher hydraulic safety and lower hydraulic efficiency (Larter et al., 2017; Maherali et al., 2004; Rosas et al., 2019; Schuldt et al., 2016; Williams et al., in review). In contrast, intraspecific responses across climate gradients have been less studied and have yielded contradictory results. Some studies have shown higher embolism resistance with decreasing water availability (Schuldt et al., 2016; Stojnić et al., 2018), while others have shown the opposite (Herbette et al., 2010) or no correlation (González-Muñoz et al., 2018; Martin-StPaul et al., 2013; Rosas et al., 2019). Indeed, drought escape strategies vary across tree life histories and their associated traits, such as reduced leaf size and number, reduced leaf growth, lowered stomatal aperture, and reduced stomatal conductance (Adler et al., 2014; Anderegg et al., 2016; Kelly et al., 2021; Tardieu and Tuberosa, 2010). The traits found in trees in drought-prone areas may not be present in trees in less drought-prone areas, which may be more affected by shifts in water availability. By investigating the responses of a riparian tree species to seasonal changes in drought along a downstream-upstream hydroclimatic gradient, we intend to better characterize the responses of trees to changing hydroclimatic conditions in areas unaccustomed to drought.

Trees use various strategies to withstand water stress. These adaptations are either morphological, physiological, or biochemical and are designed to maximize productivity while limiting water loss (Lisar et al., 2012). Tree drought strategies involve a mixture of stress avoidance and tolerance, achieved primarily through varying levels of stomatal conductance control (Tardieu and Simonneau, 1998). As drought intensifies and soil water availability decreases, trees regulate their stomatal conductance along a stringency gradient from isohydric to anisohydric (Fu and Meinzer, 2019; Martínez-Vilalta and Garcia-Forner, 2017; McDowell et al., 2008). Species tending towards isohydric behavior regulate leaf water potential (Ψ_m) more strictly by progressively closing their stomata to limit water loss. In contrast, those leaning towards anisohydricity maintain their stomata open and allow their water potential to decrease steeply with decreasing water availability. However, the degree of iso/anisohydricity is not species-dependent and appears to be strongly modulated by plant-environment interactions and can vary within the same species and even more so at broad landscape scales (Martínez-Vilalta and Garcia-Forner, 2017). Several metrics have been proposed to assess tree water status, such as midday leaf water potential, which is a common variable that measures the potential energy of water to move from roots to leaves. Relative water content (RWC) is another variable that has gained popularity because of its ease of measurement and ability to serve as a good indicator of landscape-scale mortality (Martinez-Vilalta et al., 2019). However, these variables are often limited to leaf organs and lack a more integrative value at the individual scale. To obtain information on global tree strategies in the face of drought, the intrinsic water use efficiency (WUE_i), an integrative measure of the balance between carbon uptake and water loss at

the leaf surface, can be used as a valuable indicator of how trees adapt to changing climate conditions (Weiwei et al., 2018). However, obtaining data through these ecophysiological measurements requires significant financial and time investments, especially when working at large spatial and temporal scales.

To address these challenges at broader scales, remote sensing tools have been developed to estimate vegetation water status and identify areas most affected by drought (Le et al., 2023). These tools use a range of spectral wavelengths to detect changes in the reflectance or thermal properties of plants. Vegetation indices based on reflectance in the visible or near-infrared spectrum, such as the normalized difference vegetation index (NDVI), are primarily used to estimate leaf chlorophyll content (Rouse et al., 1974), but several studies have shown significant relationships between changes in greenness and water availability (Aguilar et al., 2012; Sturm et al., 2022). In addition, the thermal radiation emitted by trees is widely used to estimate tree water status because canopy temperature is a reliable proxy for transpiration (Fuchs, 1990). Indeed, the underlying assumption is that when plants close their stomata in response to water scarcity, transpiration is reduced (i.e., lower stomatal conductance), thereby reducing the cooling effect of transpired water. Thus, the leaves of stressed plants appear warmer than those of non-stressed individuals (Jones et al., 2003, 2018; Kibler et al., 2023). The combined use of ecophysiological indicators and remote sensing, especially thermal infrared imaging, is commonplace in agronomy to assess water stress in crop plantations in environments heavily influenced by human activities (Ben-Gal et al., 2009; Berni et al., 2009). These studies demonstrated significant correlations between remotely sensed water stress indicators and ecophysiological measurements. However, this combination of tools has rarely been used to study the water stress responses of trees or forests, where the dynamics affecting water stress are more diverse and complex than those in human-dominated ecosystems. Recent studies have demonstrated the potential of these tools to assess forest water status and health at the stand scale (Marusig et al., 2020). However, to the best of our knowledge, few studies have combined these tools to assess the water stress responses of riparian forests at the landscape scale while accounting for climatic variability.

In this study, we combined ecophysiological and remote sensing measurements to assess the responses of riparian trees to seasonal drought progression at three sites across a hydroclimatic gradient. These methods were designed to provide insights into the behavior of riparian trees during drought, as well as the water stress resistance mechanisms they have developed. We also evaluated the effects of local water availability on the drought resistance of white poplars. Thus, we hypothesized that: (1) the response of trees to drought will differ according to their relative (within-site) access to water; (2) the response of trees located in drier (more southern) areas will show stronger responses to drought in both space and time; and (3) the combination of tools will provide complementary evidence for a deeper understanding of tree responses to drought.

2. Regional context and study sites

The study area focuses on the French Rhône River, a major European

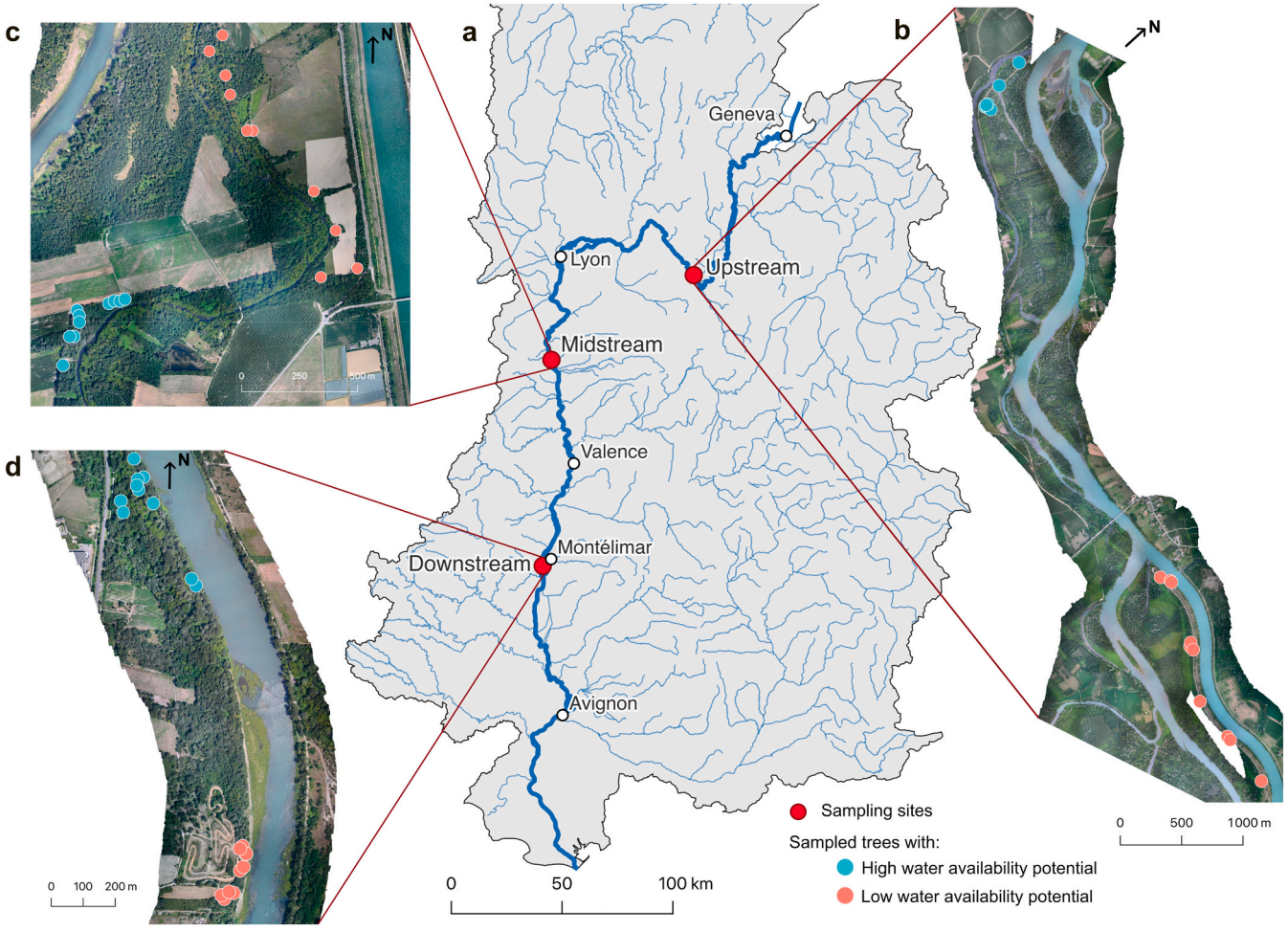

Fig. 1. (a) Location of the 3 study sites along the Rhône and of the 20 trees per site, classified according to the level of water availability (LWAP and HWAP) for (b) the upstream site, (c) the midstream site, and (d) the downstream site.

river flowing between Geneva and the Mediterranean Sea. Its catchment area covers 98,500 km^2, with a mean annual discharge of 1700 m^3/s at its mouth (Olivier et al., 2022). The river corridor is mainly north-south oriented (Fig. 1a) and characterized by an important hydroclimatic gradient, from wetter and cooler conditions in the north to drier and warmer conditions in the south (Sargeant and Singer, 2021; Sauquet et al., 2019). This hydroclimatic gradient strongly influences the growth and health of riparian trees, which are sensitive to both local and non-local climate forcing (Lochin et al., in review; Sargeant and Singer, 2021). Despite these climatic differences, riparian forests are homogeneous in species and distribution along the hydroclimatic gradient (Olivier et al., 2022). They are primarily dominated by a combination of early successional trees, including *Populus nigra*, *Populus alba*, and *Salix alba*, and post-pioneer trees, such as *Fraxinus excelsior* and *Acer platanoides* (Räpple, 2018). These forests are also home to invasive species, such as *Acer negundo* and *Robinia pseudoacacia* (Janssen et al., 2020).

The Rhône is a highly modified river that has undergone several large-scale development projects since the 19th century. The most recent and transformative project involved the construction of 16 dams and diversion canals for hydropower generation (Lamouroux et al., 2015; Olivier et al., 2022). These structures have altered hydrological, sedimentary, and ecological flows, particularly in the Old Rhône, the former main channel, where flows have been reduced by 95 % following the creation of diversion canals (Bravard and Gaydou, 2015; Vázquez-Tarrío et al., 2019). These hydrological consequences, combined with the incision of the Rhône and the lowering of water levels due to the high frequency of low minimum discharge, have led to a drop in water levels and a significant disconnection of alluvial stands (Olivier et al., 2022).

To account for hydroclimatic differences, we selected three sites (Fig. 1a) distributed along the Rhône River: Brégnier-Cordon (hereafter referred to as upstream, Fig. 1b), Péage-de-Roussillon (midstream, Fig. 1c), and Montélimar (downstream, Fig. 1d). At these three sites, mean climatic parameters during the growing season from May to August, between 1995 and 2023, showed significant differences. The mean air temperature at the upstream site was 19.1 °C (±4.1 °C), with a total precipitation of 373 mm (±96 mm). At the midstream site, these values were 20.1 °C (±4.1 °C) and 244 mm (±66 mm), respectively, whereas at the downstream site, they were 22.1 °C (±3.9 °C) and 183 mm (±76 mm), respectively (E-OBS data). In addition, to represent equivalent hydrological conditions, we selected these three sites in bypassed reaches constrained by minimum flows, each characterized by two forest stands with contrasting water availability conditions.

3. Methods

3.1. Space-time sampling framework

3.1.1. Species selection

Our study focused on white poplar (*Populus alba*) because it is one of the dominant riparian species along the Rhône River and is found both upstream and downstream (Olivier et al., 2022). White poplar is a phreatophyte species that relies heavily on root connections to the alluvial water table (Sánchez-Pérez et al., 2008; Sargeant and Singer, 2021; Singer et al., 2013), making it highly sensitive to fluctuations in water availability and a sentinel species for changes in hydrological conditions (Braatne et al., 1996; Rood et al., 2003, 2011). Several studies have demonstrated that *Populus* species can adapt their stomatal sensitivity and gas exchange characteristics to local native conditions (Bassman and Zwier, 1991; Blake et al., 1984; Dunlap and Stettler, 2001; Pearce et al., 2006). As a result, resistance and responses to water stress can vary widely among *Populus* genotypes, both inter- and intra-specifically (Gebre and Kuhns, 1993; Marron et al., 2002; Street et al., 2006).

3.1.2. Selection of forest stands and in-field trees

We aimed to select forest stands with a high or low degree of connection to groundwater, a proxy for water availability. Unfortunately, groundwater depth data were not available for all sites. Therefore, we used the mean water level of the Rhône River as a proxy for groundwater depth because it has been established as a reliable indicator of groundwater elevation near the channel (Brooks et al., 2012; Taylor and Alley, 2001). The use of this proxy was particularly appropriate for our study sites, which are adjacent to bypassed reaches where flow is highly controlled and therefore water level fluctuations are limited. We used the mean water level provided by the Compagnie Nationale du Rhône (CNR), which was interpolated over our study sites using the inverse distance-weighted method. We then used a 20 cm resolution digital terrain model (Džubáková et al., 2015) from a LiDAR campaign (BDT Rhône), which we subtracted from the interpolated water level to obtain the difference between water level and ground elevation. Areas with the lowest difference are considered to be better connected than areas with a higher elevation difference (see S.I. Fig. S1).

Based on these data, we conducted a field survey to identify two forest stands with different elevations relative to the channel at each site. The stand with the lower elevation relative to the channel was considered to be potentially better connected to groundwater and was therefore classified as having High Water Availability Potential (HWAP), whereas the stand with the higher elevation was classified as having Low Water Availability Potential (LWAP). The distribution of tree elevation relative to the channel for the two forest stands at each site (see S.I. Fig. S2) showed significant differences upstream and downstream ($p < 0.01$ and $p < 0.001$, respectively). However, at midstream, both stands have similar relative elevations (see S.I. Fig. S2), but this similarity hides a clear difference in groundwater availability. In fact, at midstream, high levels of groundwater pumping for industrial use have led to a lowering of the water table (Hydrofis-Brli, 2015; Labroche et al., 2017). According to piezometric observations and the hydrogeological model carried out by Hydrofis/BRLi, this pumping has created a cone of depression with a water table drawdown of up to 1 to 1.5 m (BRLi, 2023; Hydrofis-Brli, 2015; Labroche et al., 2017). The LWAP stand was located exactly where the pumping wells were found and where the groundwater level was lower. In contrast, the HWAP stand is located where groundwater is only marginally affected by the cone of depression (BRLi, 2023; Hydrofis-Brli, 2015).

We selected 10 trees per stand according to a diameter gradient to test the hypothesis that this variability could influence the response of white poplars to water stress (Bennett et al., 2015). We carefully selected mature trees with a mean stem diameter of 62.6 cm (±25.1 cm) at breast height and a mean height of 21.3 m (±4.9 m); more information about trees in each stand at each site can be found in S.I. (Table S1). We measured the circumferences using flexible tape and extracted tree heights from a canopy height model developed using data from the LiDAR HD program of the French National Geographic Institute (https://geoservices.ign.fr/lidarhd). Each tree was located using high-accuracy DGPS (Geomax Zenith 35 Pro). Trees were selected according to three criteria: (1) ease of access to enable regular sampling; (2) availability of low-hanging, reachable branches; (3) visibility of the entire canopy from above to ensure clear identification of trees on aerial images; and (4) location in dense forest with closed canopy cover to ensure a homogenous NDVI signal.

3.1.3. Climatic characterization of the season studied

To characterize the meteorological conditions at the three sites in 2023, we used the E-OBS gridded dataset (https://www.ecad.eu/), which provides daily weather data with a spatial resolution of 0.1° (~11 km) (Cornes et al., 2018). Specifically, we extracted the mean air temperature (TG), minimum air temperature (TN), maximum air temperature (TX), precipitation sum (RR), mean sea level pressure (PP), mean wind speed (FG), mean relative humidity (HU), and global radiation (QQ) at a daily time step between 1995 and 2023.

From these data, we calculated the daily reference evapotranspiration (ET_0) using the Penman-Monteith approach (Allen et al., 1998; Pohl

et al., 2023). We used daily ET_0 to calculate the Standardized Precipitation Evapotranspiration Index (SPEI) (Beguería et al., 2010; Vicente-Serrano et al., 2010). The SPEI is one of the most popular and accurate indices for characterizing drought conditions. A negative SPEI indicates a relatively dry climate, whereas a positive SPEI indicates a relatively wet climate compared to the mean climatic state (Vicente-Serrano et al., 2010). We computed a 30-day rolling SPEI value because it is the most commonly used timescale for identifying meteorological drought (Wang et al., 2014). The 30-day SPEI was used to estimate drought conditions in 2023 at each site and to identify different periods of drought within the growing season (Fig. 2).

Threshold analysis was performed to identify different periods of drought within the growing season. We used a threshold of SPEI < -1 to define a state of significant drought, as it is commonly employed in several studies (Ma et al., 2020, 2023; Wang et al., 2014). The growing season was divided into three distinct phases: (1) the pre-drought phase (hereafter referred to as Pre- in figures), which extended from the first sampling date to the point when the SPEI fell below −1 for at least 30 consecutive days; (2) the drought phase, characterized by SPEI values consistently below −1; and (3) the post-drought phase (hereafter referred to as Post- in figures), which began when the SPEI exceeded −1 and lasted until the last sampling date. At the three sites, the drought

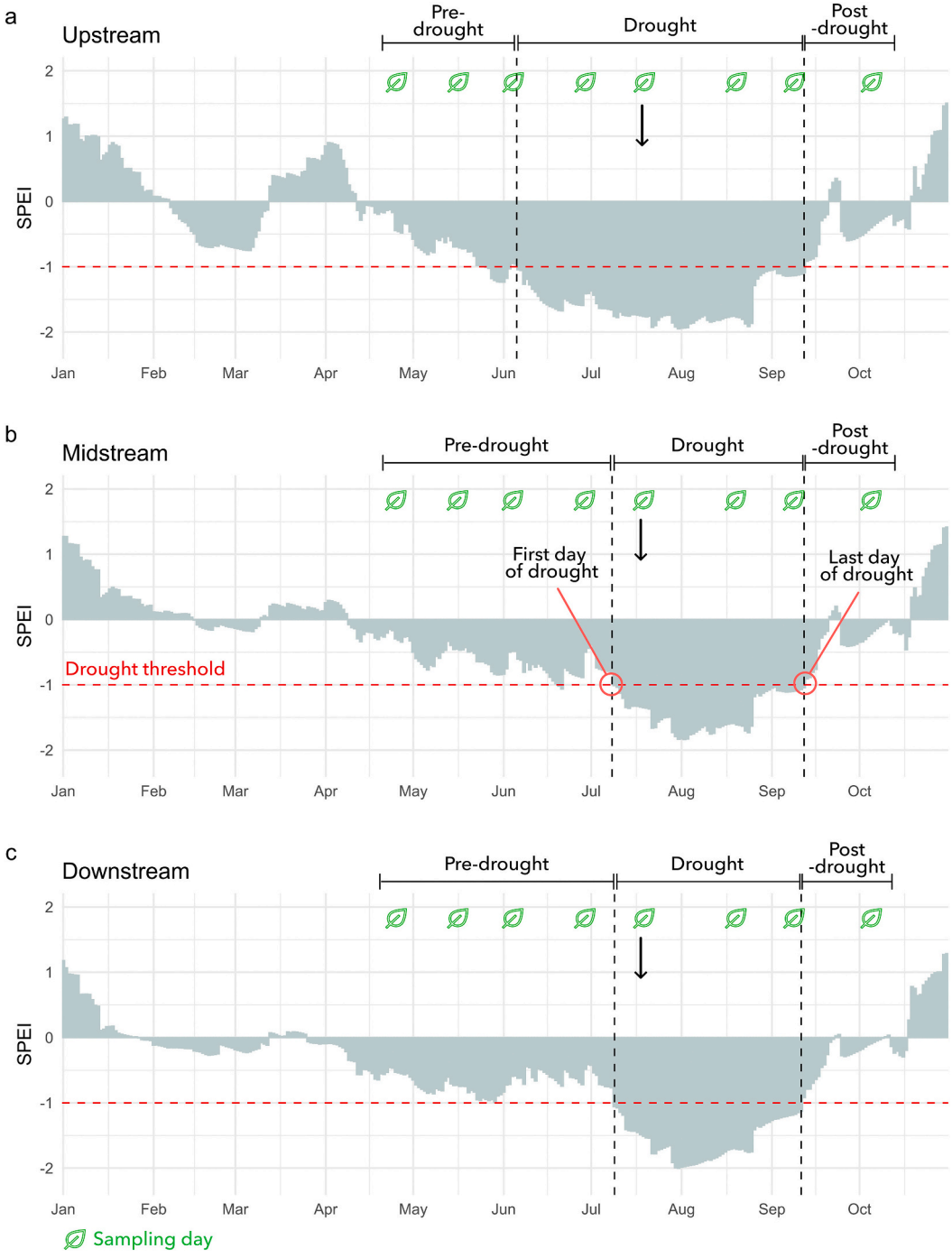

Fig. 2. Evolution of the 30-day SPEI from January 1 to October 31, 2023 at the three sites. The two black dotted lines represent the start and end dates of drought at each site, while the red dotted line represents the drought SPEI threshold. Green leaves indicate the days on which samplings were conducted, and black arrows indicate the thermal survey.

onset dates differed (Fig. 2), indicating an earlier drought onset in the upstream reach (158 DOY, June 7; Fig. 2a) than in the midstream (190 DOY, July 9; Fig. 2b) or downstream reaches (190 DOY, July 9; Fig. 2c). The pre-drought phase begins with our first sampling date and the post-drought phase ends with our last sampling date (see S.I. Table S2).

3.2. Ecophysiological field measures

3.2.1. Leaf traits

During the growing season, we measured the minimum leaf water potential (Ψ_m, MPa) every three weeks at all sites and in each forest stand. We collected a live poplar branch with leaves from the lower canopy (between 2 and 7 m above the ground) from each tree between 11:00 a.m. and 2:00 p.m. Next, we selected two green leaves and placed them in an aluminum bag with wet paper inside to maintain high humidity levels under dark conditions. Finally, we stored the branches in a cooler box until measurements at the lab, approximately 3 h later. Ψ_m was determined for each selected leaf using a pressure chamber (mod. 1505D, PMS Instrument Company, Albany, OR, USA 1505D), (Scholander et al., 1965). The mean of the two measured leaves per tree was then used as a single replicate for each tree and sampling date. Some trees became inaccessible during the campaign because of broken branches or branch mortality, so the number of replicates varied between sites and dates. The number of samples obtained at each site for each sampling date is summarized in Table S2 (see S.I.).

On each sampling date, ten additional green leaves were collected from each tree. These leaves were weighed in the laboratory in three stages: (1) fresh weight (FW, g), (2) turgid weight (TW, g) measured after immersing the petiole in water for 12 h, and (3) dry weight (DW, mg) after drying in an oven at 80 °C for 48 h after the first two measurements. Using FW and DW, we calculated the leaf dry matter content (LDMC, mg g^{-1}) as follows (Pérez-Harguindeguy et al., 2016):

$$LDMC = \frac{DW}{FW} \quad (1)$$

Relative water content (RWC, %) was calculated according to the formula developed by Smart and Bingham (1974):

$$RWC = \frac{FW - DW}{TW - DW} \quad (2)$$

3.2.2. Phloem sampling and $\delta^{13}C$ analysis

Phloem was sampled simultaneously with leaf sampling in each forest stand and at each of the three sites. All trees were sampled. A detailed field protocol has recently been published describing all steps to consider (Gerle et al., 2023). We provide a summary here.

Phloem discs were collected at breast height using a 9 mm diameter cork-borer. The bark and wood were carefully removed to isolate the active phloem, which was then immersed in an exudation solution. The carbon stable isotope ratio of the exuded phloem content was measured at the LEHNA "Isotope Ecology" platform using an isotope ratio mass spectrometer (Isoprime 100, Elementar) coupled in continuous flow to an elemental analyzer (Vario PyroCube, Elementar). Isotope ratios were expressed as $\delta^{13}C$ in ‰ relative to the Vienna Pee Dee Belemnite (VPDB). The IAEA-CH3 and IAEA-CH6 reference materials were analyzed with the samples, and the standard deviations of the replicate analyses were lower than 0.20 ‰.

From the $^{13}C/^{12}C$ ratio, we calculated the isotopic discrimination against ^{13}C (Δ, ‰) and intrinsic water use efficiency (WUE_i, μmol CO_2 mol H_2O^{-1}), following calculations detailed in Vernay et al. (2020, 2024). Two differences occurred compared to the cited literature: for Δ calculation, we used a constant $\delta^{13}C_a$ because it can be considered as a constant value of −8 ‰ at mid-latitudes (Yakir and Sternberg, 2000), and for WUE_i, we also used a constant g_s/g_m, increasing the accuracy of WUE_i estimates (Vernay et al., 2020). Although we did not estimate this ratio in this experiment, we used a value of 0.51 determined on poplar species (Théroux-Rancourt et al., 2014).

3.3. Satellite remote sensing acquisition and processing

Sentinel-2 satellite imagery was used to assess the vegetative response of individual trees over time. These satellites provide imagery with a spatial resolution of 10–20 m and a temporal resolution of six days over the study area (Li and Roy, 2017). All available bottom-of-atmosphere images (Level 2A) with a cloud cover of <30 % were used and processed using a cloud mask. These images were acquired and processed using Google Earth Engine (Gorelick et al., 2017). They were used to calculate the Normalized Difference Vegetation Index (NDVI) at a spatial resolution of 10 m to assess and quantify the health of riparian tree canopies during the growing season. This indicator provides global and regular information on the evolution of canopy health in the stands studied, allowing us to assess whether NDVI is a reliable indicator of tree water status.

The NDVI was calculated using the following formula:

$$NDVI = \frac{NIR - R}{NIR + R} \quad (3)$$

where NIR corresponds to Sentinel-2 satellite band 8 and R corresponds to the visible red band (i.e., band 4). The median NDVI values were extracted from the canopy of each sampled tree. Canopy polygons were delineated using the method described in Section 3.4. In total, we obtained an NDVI time series for the growing season of 2023, consisting of 168 images covering the three sites.

3.4. Airborne remote sensing acquisition and processing

Aerial imagery was collected using an ultralight trike. Two cameras were carried during the flight to collect visible (RGB) and thermal infrared (TIR) data. The cameras were mounted on a stabilizer to provide clear images despite the motion induced during the flight. Each camera was programmed in time-lapse mode to capture an image every 2 s and was connected to an external battery and a laptop to be operated in flight to adjust the focus, if necessary. The visible camera was a Nikon Z 6 II (30 mm lens) with a resolution of 6048 × 4024 pixels and was connected to a GPS transmitter. The thermal infrared camera was a VarioCam HD head with a resolution of 1024 × 768 pixels, which senses infrared radiation in the 7.5–14 μm range. Each site was overflown between 11:30 a.m. and 12:30 p.m. on July 12 (downstream), 17 (upstream), and 18 (midstream), concomitantly with ecophysiological campaigns, on days with clear skies and no precipitation during the previous 24 h. The average flight altitude was 500 m above ground level, resulting in visible images with resolutions of 6 cm·pixel^{-1} and 30 cm·pixel^{-1} for the TIR images.

Each set of images was processed separately using Agisoft Metashape Professional 2.0.2 software. First, geotagged RGB images were imported into the software in their original format (.jpeg) and aligned. Then, alignment was optimized in QGIS (3.32) using markers based on the latest IGN Ortho 20 cm orthophotos and IGN high-resolution LiDAR. The generated orthophoto had a resolution of 6 cm. To generate the final thermal orthomosaic, thermal images were first aligned using existing GPS information and then carefully aligned on the previously generated orthophoto. The exported thermal orthomosaics consisted of a single band (temperature in Kelvin) converted to °C with a resolution of 30 cm·pixel^{-1}.

Considering that it is preferable to measure canopy temperature by averaging all leaves (Jones et al., 2009), we extracted the mean value of the entire canopy for each tree. The canopy of each sampled tree was delineated using its exact GPS location, high-resolution orthophotos, and canopy height model. Based on the GPS coordinates and the canopy height model, we identified the crown of each tree, which was then manually delineated using QGIS. To validate crown delineation, we

visually compared them to the high-resolution orthophotos. Extraction from these polygons resulted in 60 values (20 per site) of the mean canopy temperature (T_c). We then calculated the canopy temperature relative to air temperature ($\Delta T_{c\text{-}a}$) using air temperature (T_a) from the nearest weather station at each site at the time of the flight. This standardization allowed us to account for climatic differences between sites and flights and is considered a reliable estimator of tree water use (Gonzalez-Dugo et al., 2012; Hernández-Clemente et al., 2019; Lapidot et al., 2019).

3.5. Statistical analysis

To facilitate data analysis, we averaged each variable by site and stand. To this end, we tested whether diameter variability could influence the variance of ecophysiological measurements and, if so, introduced diameter as an explanatory variable. To assess the variance of WUE_i and Ψ_m we performed a linear mixed effects analysis using the lme4 package (Bates et al., 2012) in R, which was used to perform all the analyses and statistical tests (R Core Team, 2022). The dependent variable was WUE_i or Ψ_m, and diameter, stand, and drought period (pre-drought, drought, and post-drought) were used as fixed effects. To account for multiple sites, site was entered as a random effect.

The relationship between leaf traits (Ψ_m, WUE_i, RWC, and LDMC) and drought period was also tested using linear mixed effects analysis to compare means at each site in each drought period. Drought periods (pre-drought, drought, and post-drought) and sites (with interaction terms) were entered into the model as fixed effects. Drought periods (Period) and trees were used as random effects to account for repeated measurements (Trait ~ Period*Site + (Period | Tree)). Visual inspection of residual plots did not reveal any obvious deviations from homoscedasticity or normality. Based on the model, we then performed post-hoc pairwise comparisons for each leaf trait using Tukey's estimated marginal means with the emmeans R package (Lenth, 2023). Post-hoc tests were performed for pairwise comparisons of the means for each leaf trait (RWC and LDMC) across sites (upstream, midstream, and downstream).

Finally, post-hoc pairwise comparisons of mean NDVI between each drought period (pre-drought, drought, and post-drought) and each forest stand (LWAP and HWAP) were calculated using a linear mixed model to account for repeated measures. The same procedure was used for canopy temperatures.

4. Results

4.1. Multi-date ecophysiological analysis through the season

Analysis of the dynamics of the minimum leaf water potential (Ψ_m) during the growing season showed a similar seasonal pattern among sites (see S.I. Fig. S3a). Ψ_m decreased from the beginning of the growing season and reached a minimum in late August and early September, before increasing at different rates among sites and forest stands. Diameter analysis indicated that diameter had a significant effect on Ψ_m ($F(1,136) = 14.2$, $p < 0.001$), with higher Ψ_m as diameter increased. A similar seasonal pattern was observed for WUE_i at all three sites (see S.I. Fig. S3b), with a slight increase from the beginning of the growing season to July, followed by a decrease to a minimum in late August and early September. Finally, WUE_i appeared to increase again at the last

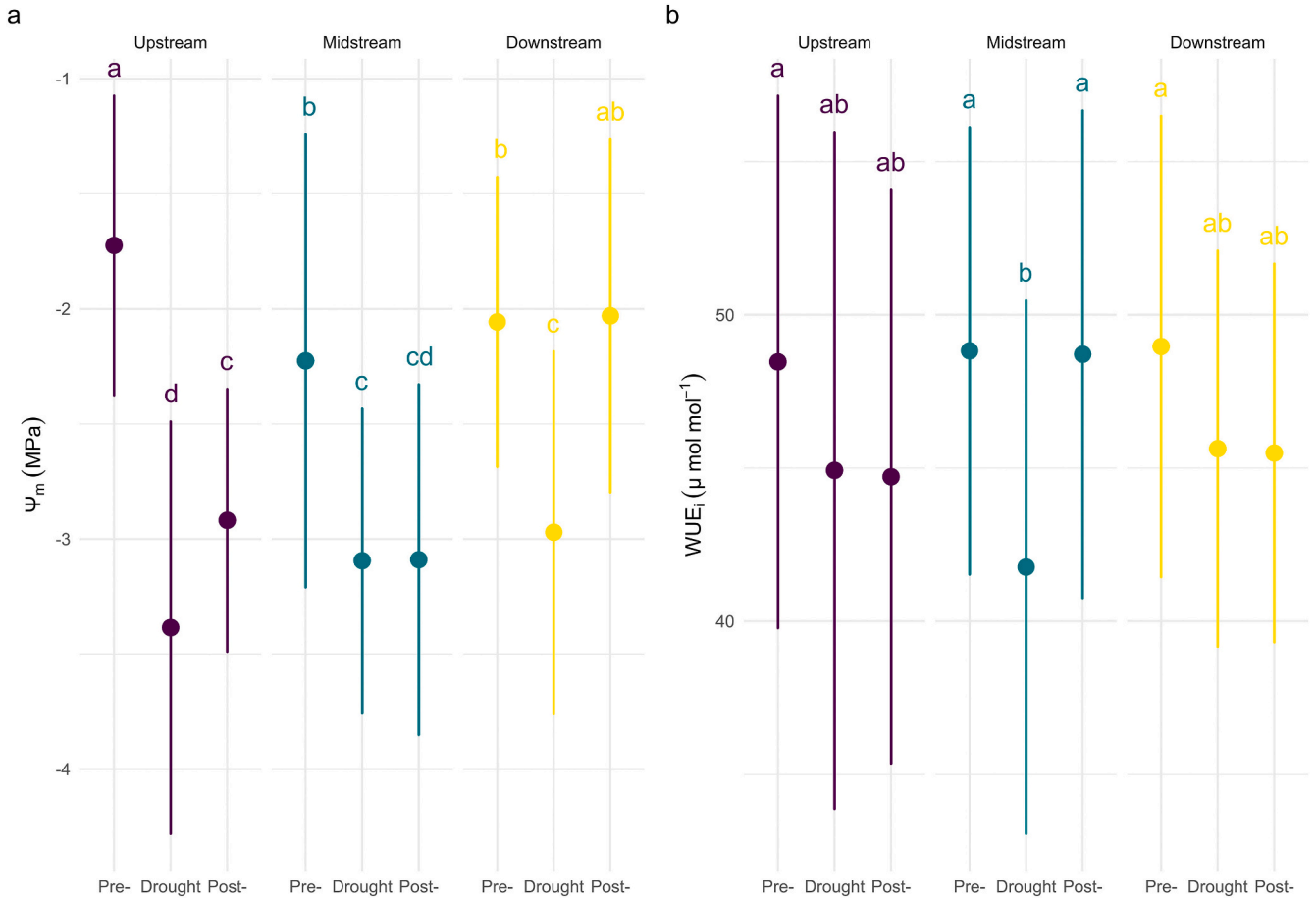

Fig. 3. Means and standard deviations of (a) minimum leaf water potential (Ψ_m) and (b) intrinsic water use efficiency (WUE_i) over each drought phase among the three sites. Colors indicate site identification only. Means by sites and periods without common letters were significantly different at the 95 % confidence level ($p < 0.05$) in Tukey's HSD post hoc tests.

sampling date. The diameter had no significant effect on the variance of WUE_i ($F(1,203) = 0.42$, $p = 0.52$).

Overall, differences in water availability conditions (HWAP and LWAP) at each sampling date did not significantly affect the variability of Ψm ($F(1,18) = 0.27$, $p = 0.61$) and WUEi ($F(1,18) = 0.02$, $p = 0.89$). Therefore, we further assessed their seasonal dynamics by focusing primarily on the variability between sites (Fig. 3) rather than within sites (i.e., HWAP/LWAP).

The seasonal pattern of Ψ_m during the different phases of drought showed significant differences between the sites (Fig. 3a). Pre-drought Ψ_m values were significantly higher upstream than downstream and midstream. After the pre-drought phase, a significant decrease in Ψ_m occurred during the drought phase, but the magnitude of the change differed between the sites. A minimum value (−3.38 MPa) was found upstream, which was significantly lower than that of the other two sites. This inter-site difference was also observed in the post-drought phase, where downstream Ψ_m was significantly higher than upstream and midstream Ψ_m, indicating that Ψ_m recovered to pre-drought levels only at the downstream site.

The seasonal pattern of WUE_i (Fig. 3d) was similar at the upstream and downstream sites, with WUE_i gradually decreasing throughout the growing season, but was highly contrasted at the midstream site. Pre-drought WUE_i values were not significantly different among the three sites. Then, between pre-drought and post-drought, a significant decrease was observed at all sites, but was more pronounced at the midstream site. After the drought, upstream and downstream WUE_i remained low, while midstream WUE_i returned to pre-drought levels. Although patterns and means were not significantly different between upstream and downstream, variability was higher upstream than downstream, indicating that individual trees did not respond uniformly throughout the growing season.

Fig. 4 provides further evidence that white poplars did not behave similarly along the hydroclimatic gradient throughout the season. Leaf dry matter content (LDMC) remained higher upstream ($p < 0.001$) throughout the growing season (Fig. 4a). Similarly, the seasonal pattern of LDMC showed significant differences in mean values between

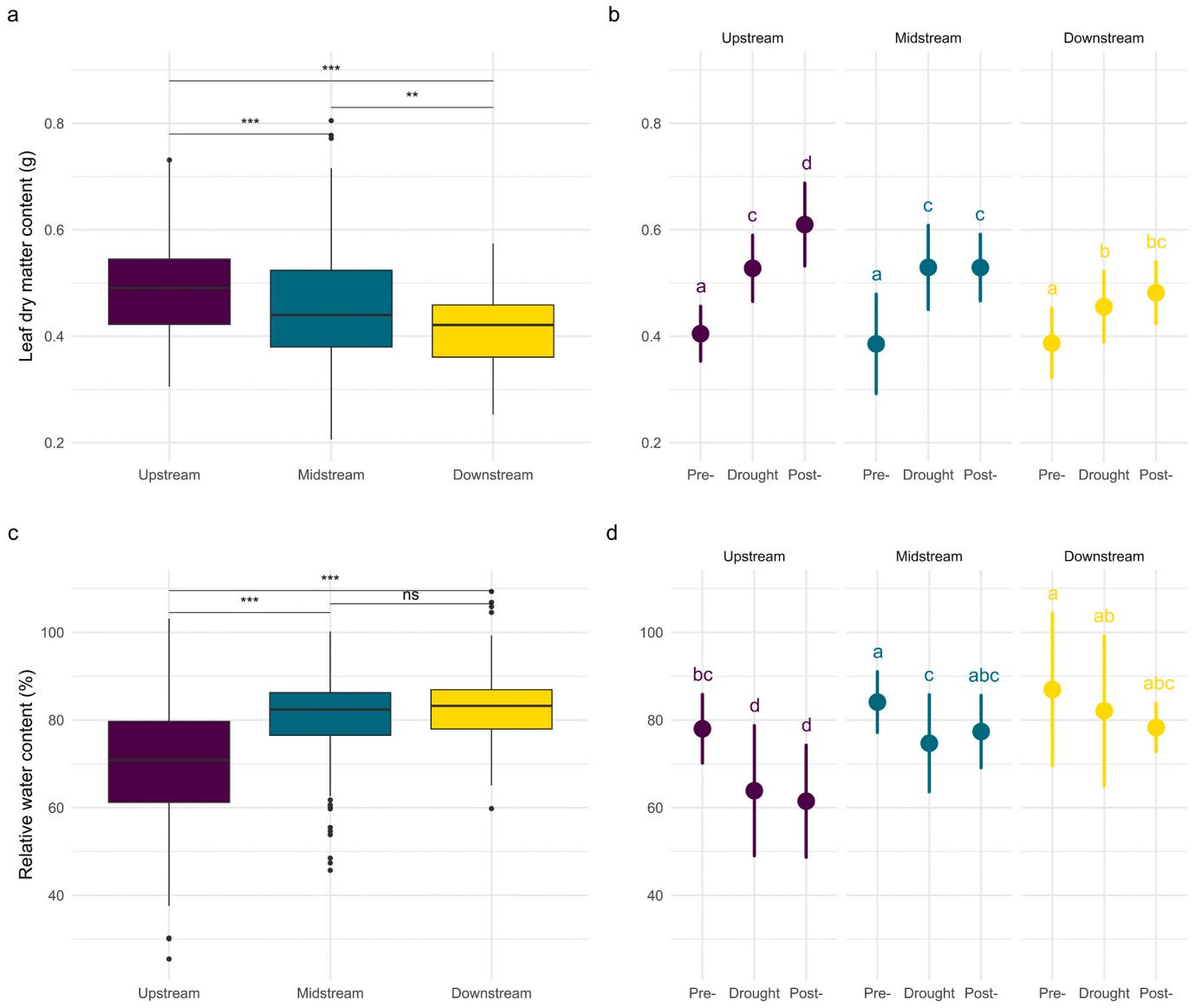

Fig. 4. Boxplots of (a) leaf dry matter content (LDMC) and (c) relative water content (RWC) by site (upstream, midstream, downstream). Mean and standard deviation of (b) LDMC (d) and RWC for each drought phase and site. Colors are for site identification only. * indicates that the difference between means of each site is statistically significant according to post-hoc pairwise comparison, where *** indicates $p < 0.001$, ** = $p < 0.01$, * = $p < 0.05$, and ns = $p > 0.05$. Means without common letters were significantly different at the 95 % confidence level ($p < 0.05$) in Tukey's HSD post hoc tests.

upstream and downstream sites in each phase (except for pre-drought) (Fig. 4b). Between pre- and post-drought, LDMC increased by 53 % upstream, compared to 42 % midstream and 35 % downstream. The same observation holds for the relative water content (RWC, Fig. 4c). Leaves at the upstream site contained less water than those at the midstream ($p < 0.001$) and downstream sites ($p < 0.001$) but there was no significant difference between the midstream and downstream sites ($p = 0.089$).

Median RWC over the entire growing season was 71 % at the upstream site compared with 82 % and 83 % at the midstream and downstream sites, respectively. Seasonal trends in RWC (Fig. 4d) showed a decreasing trend throughout the growing season at the upstream site, with a significant difference between pre-drought and drought, and relative stabilization in the post-drought period. The pattern was similar at midstream, with a significant decrease between pre-drought and drought, followed by a non-significant increase. At the downstream site, no significant difference in RWC was observed between each drought phase. Upstream, RWC decreased by approximately −28 % between pre- and post-drought, whereas it decreased by only −9 % midstream and −7 % downstream.

4.2. Seasonal-scale NDVI pattern

NDVI analysis revealed distinct seasonal patterns along the hydroclimatic gradient (Fig. 5), with significant variation between drought phases at each site ($F(4,1906) = 7.62$, $p < 0.001$). Pairwise comparisons revealed that the downstream site showed a significant decrease ($p < 0.001$) in NDVI values between pre-drought and drought, and then a slight but significant increase until the post-drought period ($p = 0.013$). At midstream, there was a significant decrease between pre-drought and drought ($p < 0.001$), followed by a stabilization after the drought ($p = 1$). Upstream, the situation was more homogeneous, with a stabilization between each phase ($p = 0.24$, $p = 0.35$). Overall, during the growing season, NDVI decreased significantly between the pre-drought and post-drought periods at all sites.

The dynamics of mean NDVI were not significantly affected by differences in water availability between forest stands ($F(4,1900) = 1.93$, $p = 0.10$). Specifically, only the downstream site showed significant differences between HWAP and LWAP for the drought and post-drought phases ($p < 0.001$ and $p = 0.003$, respectively), with NDVI values significantly higher when water was potentially available (HWAP > LWAP).

4.3. Single-date thermal pattern during the drought peak

Analysis of canopy temperatures at the three sites showed two distinct trends (Fig. 6). First, canopy temperatures were higher than air temperatures only at midstream and downstream sites, while they were lower upstream. Second, only the downstream site showed significant differences in canopy temperatures between LWAP and HWAP plots ($p = 0.002$). In contrast, variability in water availability did not seem to affect canopy temperatures, as there were no significant differences in temperatures between HWAP and LWAP upstream ($p = 0.63$) and midstream ($p = 0.48$). Downstream, canopy temperatures were higher in the LWAP plot with a median of 28.6 °C compared to 27.9 °C in the HWAP plot. Upstream and midstream canopy temperatures in the LWAP

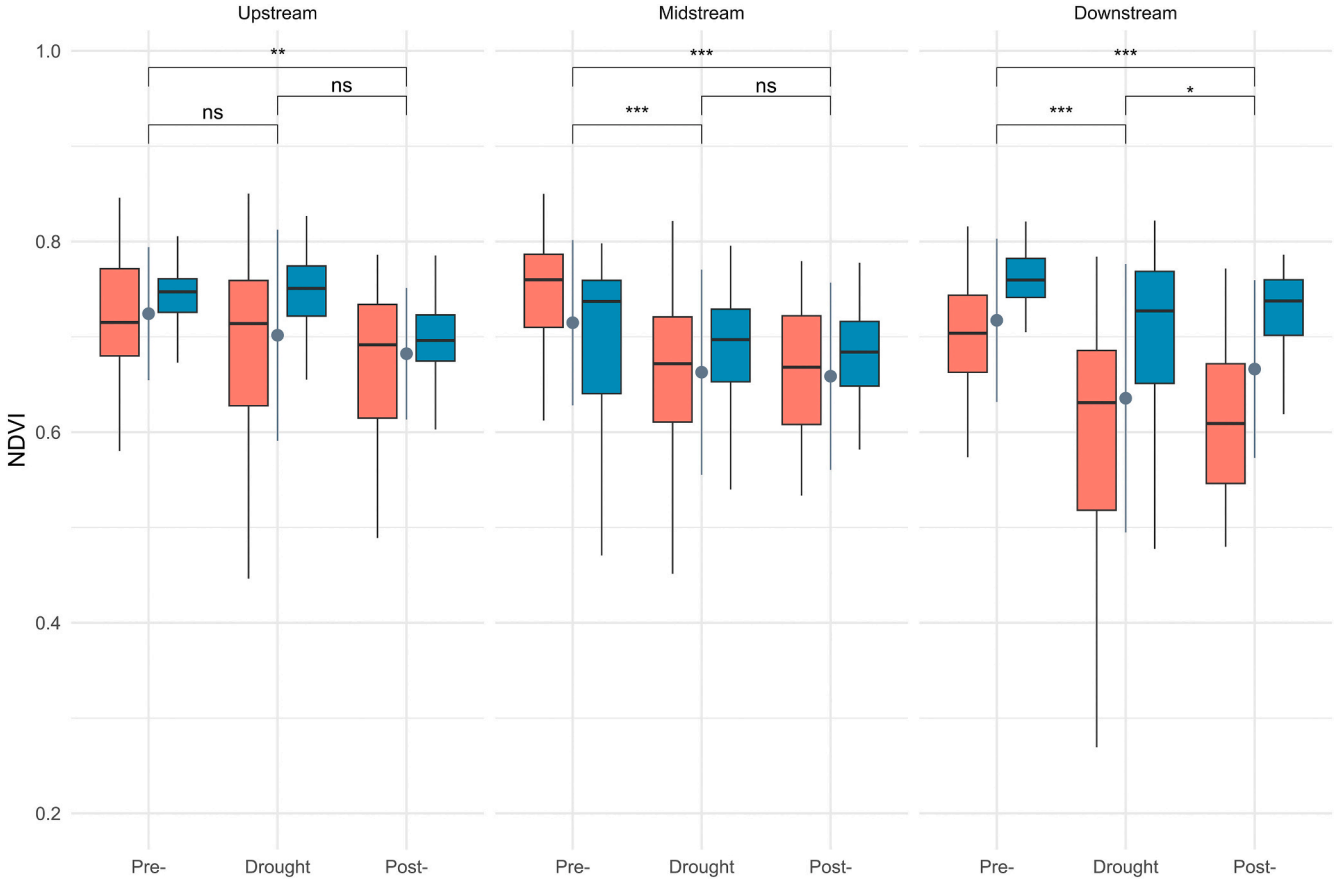

Fig. 5. NDVI boxplots over the three drought phases (Pre-drought, Drought, Post-drought) between each forest stand (LWAP in red and HWAP in blue) and each site (upstream, midstream, downstream). Gray dots indicate the mean NDVI per site and drought phase, gray bars indicate the standard deviation. * indicates that the difference between means of each drought phase is statistically significant according to post-hoc pairwise comparison, where *** indicates $p < 0.001$, ** = $p < 0.01$, * = $p < 0.05$, and ns = $p > 0.05$.

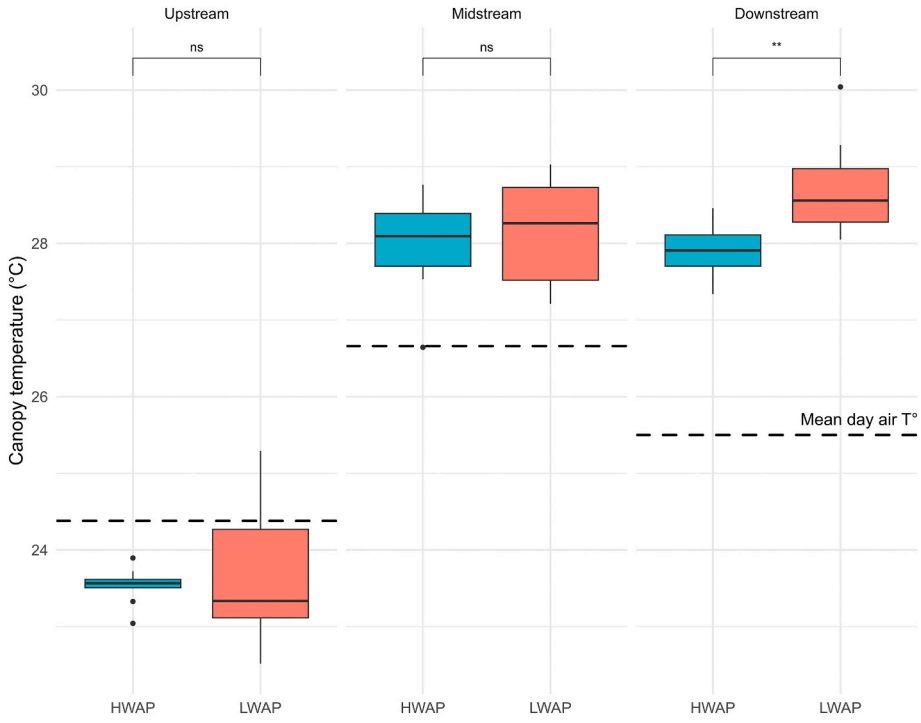

Fig. 6. Box plots of canopy temperature for each site (upstream, midstream, downstream) and plot (HWAP and LWAP). Black dashed lines represent the mean daily air temperature at the time of the survey.

plots had higher variability (1.1 °C and 0.7 °C, respectively) than those in the HWAP plots (0.2 °C and 0.6 °C).

The difference between canopy temperature and air temperature ($\Delta T_{c\text{-}a}$, Fig. 7) was significant among the three sites ($F(2,55) = 130.4$, $p < 0.001$). Only the upstream site had a negative $\Delta T_{c\text{-}a}$, indicating that the canopy temperature was lower than the air temperature. In contrast, the other two sites had positive $\Delta T_{c\text{-}a}$ values, which were highest at the southernmost site. The relationship between $\Delta T_{c\text{-}a}$ and Ψ_m clearly showed a difference between the means of the three sites, with higher canopy temperatures for higher leaf water potential (Fig. 7a). In other words, trees with warmer canopy, i.e. lower evapotranspiration rates, had higher leaf water potential. The trend was less pronounced for WUE_i, but we also observed that higher canopy temperatures resulted in lower WUE_i (Fig. 7b).

When considering all individuals (with sites as a random factor) and relating them to ecophysiological metrics, we observed a significant relationship between $\Delta T_{c\text{-}a}$ and WUE_i ($F(1,54) = 8.17$, $p = 0.006$), indicating that higher relative temperatures were associated with lower WUE_i for each individual. An opposite pattern was found for Ψ_m, with a non-significant relationship with $\Delta T_{c\text{-}a}$ ($F(1,53) = 0.89$, $p = 0.35$).

5. Discussion

Our study revealed contrasting responses of riparian trees to water stress, depending on the metrics used and the scale of measurement, summarized in a conceptual model (Fig. 8). At the canopy scale, downstream trees are more responsive to drought than upstream and midstream trees, with lower greenness (Fig. 3). However, ecophysiological metrics indicate an opposite trend, with metrics converging towards higher water stress in upstream trees than in those further downstream (Figs. 4 and 5). These different responses may reflect differences in the overall behavior of trees in the face of drought and water scarcity, depending on their life history and their hydraulic traits (Anderegg et al., 2016). This is evidenced by canopy thermal characteristics, which indicate significantly different levels of evapotranspiration among the three sites (Fig. 7).

5.1. Different drought strategies explain contrasting riparian tree responses

The significant differences observed among the three sites in both ecophysiological metrics (Figs. 3 and 4) and remote sensing metrics (Figs. 5 and 6) indicated that white poplars have contrasting responses to drought along a climate gradient (Fig. 8). This intraspecific variability contrasts with other large-scale studies on upland forests, which have found drought responses to be predominantly species-dependent (Gazol et al., 2020; Kang et al., 2024). Specifically, in riparian forests, drought response strategies are also species-dependent (Portela et al., 2023; Szatniewska et al., 2022), although Gomes Marques et al. (2018) have shown that alder trees in Mediterranean riparian forests have constant growth resilience despite increasing drought frequency. These studies have demonstrated significant functional differences between species, resulting in behavioral differences that lead to variable responses to water stress. These functional differences provide some species with better short-term resistance to water stress because they adopt isohydric regulation, which regulates stomatal closure and thus limits the risk of hydraulic failure. Conversely, less resilient species adopt anisohydric regulation, which does not regulate stomatal closure during drought, thus releasing more water through transpiration and increasing their susceptibility to hydraulic failure (McDowell et al., 2008). Our results, which considered the response of trees through the lens of both ecophysiological and thermal indicators, showed a response gradient of white poplar to water availability. Indeed, we found that trees of the same species at the upstream site primarily used anisohydric regulation because they had low leaf water potential (Fig. 4a) and canopy temperature lower than air temperature, indicating high transpiration rates (Figs. 6 and 7a). In contrast, the same data indicate that trees at the downstream site have a higher and more stable leaf water potential throughout the drought, as well as lower transpiration rates (Higher canopy temperature, Fig. 6), characteristic of a reduction in stomatal conductance and therefore of isohydric behavior.

This intraspecific variation along the hydroclimatic gradient differs from the results of other studies that have shown no variation in

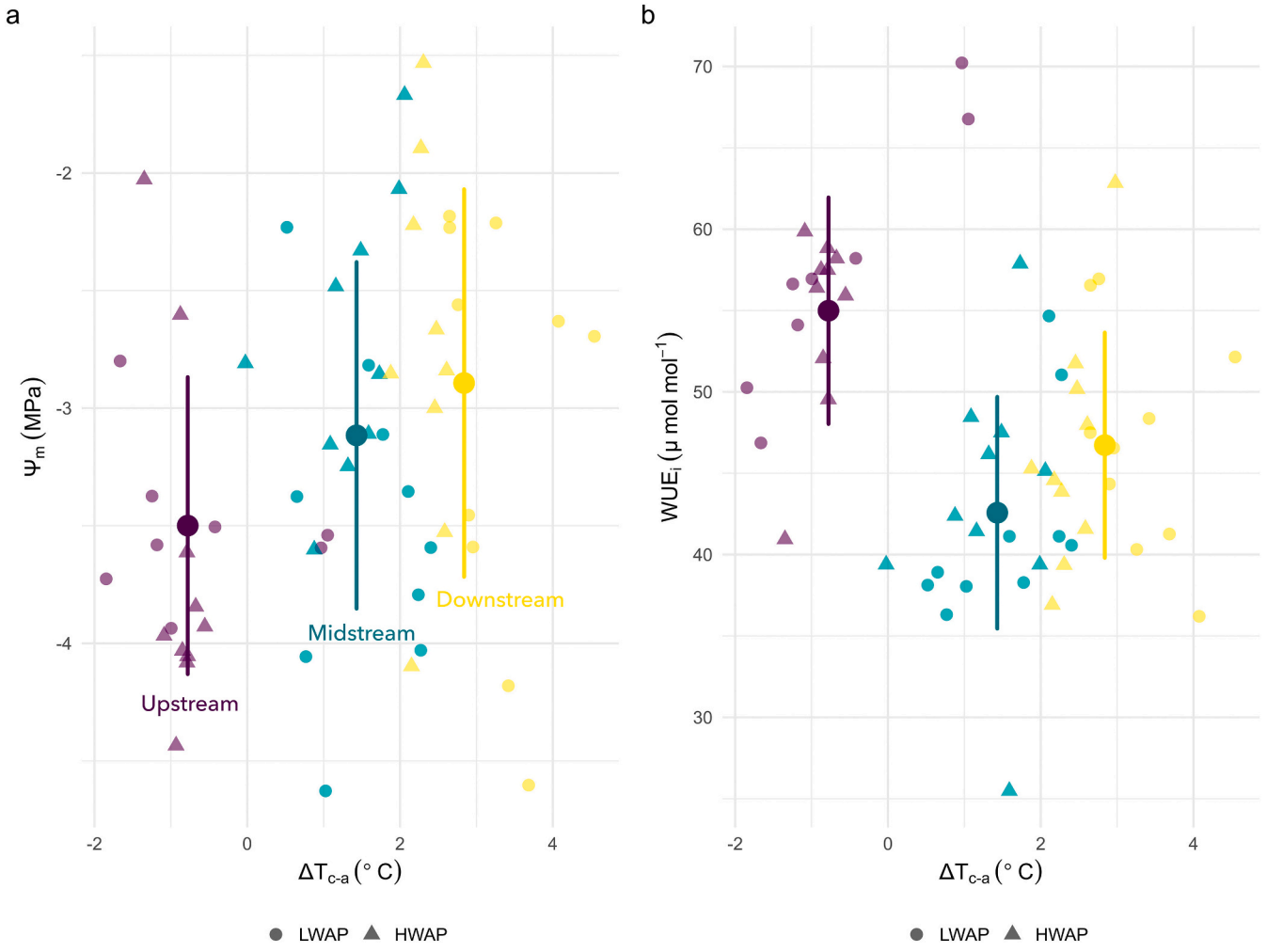

Fig. 7. Scatterplot of (a) minimum leaf water potential and (b) water use efficiency against the difference between canopy temperature and air temperature (ΔT_{c-a}) for each site (upstream, midstream, downstream). Small dots represent individual values for each tree, while large dots represent site averages. Differences in shape represent the forest stands of each individual. Colors are for site identification only.

embolism resistance within a single species along water availability gradients (Fuchs et al., 2021; González-Muñoz et al., 2018; Martin-StPaul et al., 2013; Rosas et al., 2019). However, some large-scale studies have shown that trees, such as European beech, are more resistant to embolism at the driest sites (Schuldt et al., 2016; Stojnić et al., 2018). Similarly, in riparian forests, Keller et al. (2011) showed that the traits of balsam poplar (*Populus balsamifera*) were significantly correlated with geographic location and climate, with populations in the driest areas showing better adaptation to drought than those in more humid climates. This intraspecific variability is evident at the stand level but is more nuanced at the individual level, where more heterogeneous responses are observed. This was the case for WUE_i, where upstream trees showed heterogeneous responses compared to downstream trees (Fig. 4b). Some upstream trees had WUE_i values close to those of downstream trees, indicating a significant response gradient among individuals, which limits our ability to generalize. According to some studies, this inter-individual variability in ecophysiological metrics can be explained by variability in soil water-holding capacity (Baker et al., 2019; Fuchs et al., 2021; Nie et al., 2021), tree age and diameter (Nolan et al., 2021), and neighbor competition for water (Crouchet et al., 2019). However, our results showed that water availability did not significantly affect the leaf water potential or water-use efficiency. Conversely, diameter was found to have a significant influence on tree response to water potential, with higher potential when trees have a larger diameter. This relationship may partly explain why upstream trees, that have a smaller diameter than the other two sites, have a lower water potential. This result is in line with those of Portela et al. (2023), who showed that taller riparian trees had better drought resistance and suggested that this may be explained by a deeper, more developed root system of taller trees, allowing them to reach deeper and more sustainable groundwater.

5.2. *Adaptation and plasticity of poplars to local climatic conditions*

The response and behavior differences of white poplar to drought can be explained by two interrelated hypotheses, which occur on different time scales. In the short term, the regulation of tree stomatal conductance has been shown to be highly correlated with soil and atmospheric water availability (Ruehr et al., 2016). The downstream site is influenced by a semi-arid climate with low summer precipitation and experienced a very dry beginning of 2023 (Fig. 2), reducing recharge of the vadose and phreatic zones. These lower levels of water availability at the downstream site may explain the implementation of isohydric regulation from the onset of the drought compared to the upstream site. In contrast, upstream trees benefit from higher water availability, allowing them to delay stomatal closure, and thus avoid the implementation of isohydric regulation.

The second hypothesis is also related to climatic conditions but on longer time scales. It is based on the plasticity of trees to adapt to specific environmental conditions. Downstream trees growing in a more arid

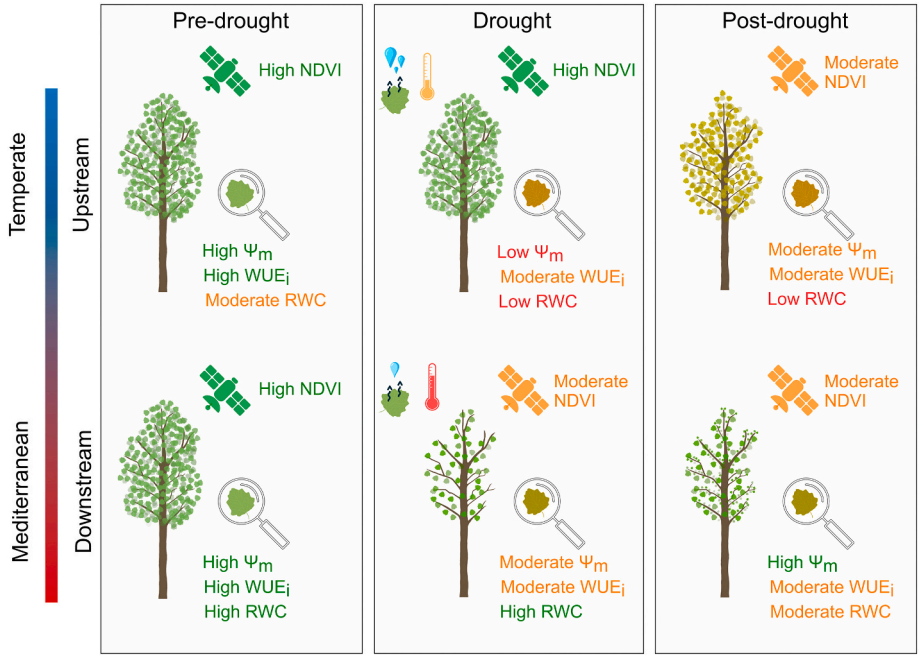

Fig. 8. Conceptual model of white poplar responses to seasonal drought development at upstream and downstream sites. Upstream white poplars exhibit high transpiration rates, resulting in low leaf water potential and water content but high NDVI. In contrast, downstream trees have low transpiration rates, resulting in higher leaf water potential and water content, but lower NDVI.

climate (e.g., under Mediterranean influence) are particularly exposed to long, intense drought episodes. However, the functional traits of trees, such as leaf area, leaf density, or branch conductivity are strongly linked to abiotic conditions (Stojnić et al., 2018), and it has been shown that aridity has the greatest impact on leaf functional traits (Salazar Zarzosa et al., 2021). Therefore, white poplars at the downstream site have a different adaptive history than upstream white poplars, which are less exposed to drought conditions (see S.I. Fig. S4). This difference in leaf functional traits enables downstream trees to respond to drought earlier and adopt more resilient behavior in the long term. Physiological trait plasticity has been demonstrated in black poplar (Fichot et al., 2024; Garavillon-Tournayre et al., 2018), but few studies have focused on white poplar. Viger et al. (2016) showed significant natural variation in phenotypic responses of black poplar in the face of drought, suggesting their adaptation to local climatic events. Similarly, a study showed that 13 stands of European black poplar had morphological and genetic traits that were dependent on adaptive differentiation and historical local events (DeWoody et al., 2015). These differences in functional traits lead to significant variability in response to drought, which can only be properly considered and measured by combining multiple tools at different temporal and spatial scales.

5.3. *Benefits of combining methods and metrics*

What emerges from these contrasting responses along the hydroclimatic gradient, and from considering the measurement tools, is the importance of adopting a holistic perspective. While remote sensing provides a comprehensive view of integrative canopy responses, ecophysiological measurements offer specific insights into the physiological mechanisms involved in tree responses. These two measurement scales are important for improving our knowledge and ability to predict drought-induced tree mortality. Indeed, our results showed that by considering only ecophysiological metrics, we were only observing part of the phenomenon related to the physiological response and stomatal regulation strategy implemented by the trees in the face of drought. Using NDVI time series, we were able to monitor the vegetative health of trees and to look at their response to drought throughout the season. In the field, we observed pronounced leaf loss in poplars at the downstream site, which seemed to contradict observations made with ecophysiological measurements. This leaf loss in downstream trees is consistent with observations made on poplars in controlled environments, where the driest sites exhibit higher leaf loss (Larchevêque et al., 2011). The use of NDVI allowed us to understand and measure this phenomenon accurately; however, this insight into the global canopy response depends on stand characteristics (forest homogeneity and density), and the resolution of Sentinel 2 satellites may limit this insight if these requirements are not met.

Without this insight into the global canopy response, our understanding of tree responses to drought would be more limited. The use of ecophysiological measurements alone revealed a more pronounced response of upstream trees to drought, which are at high risk of hydraulic failure due to low leaf water potential and leaf water content. In contrast, the use of NDVI alone showed that upstream trees had stable NDVI values during the growing season, in contrast to downstream trees. These results could lead us to two different hypotheses about the drought response of white poplar along the hydroclimatic gradient. However, their combined use allowed us to shed light on the observed differences in response and, most importantly, to gain insights into a possible explanation by a difference in behavior. Thus, using NDVI as a proxy for canopy health allows us to test whether or not tree water status is reflected in canopy health. This explains why we used this index over other indices that are better proxies for tree water status, as demonstrated by Marusig et al. (2020), using the Normalized Difference Water Index (NDWI, using SWIR band). Without a proxy for canopy health, our ability to detect differences in behavior would have been limited, and it would have been difficult to develop our hypothesis regarding differences in intra-specific behavior as a function of local climatic context.

The use of thermal infrared remote sensing confirmed these hypotheses during a single observation during drought. Compared to NDVI, its use provides information with a higher spatial resolution than satellite remote sensing, but above all, it provides a reliable proxy for transpiration and thus for the water status of trees in real-time. NDVI, on the other hand, is limited in its ability to indicate water status in real-time and to observe the consequences of the tree water status over

time, but remain a crucial indicator of tree canopy health. Thermal infrared remote sensing, if performed under optimal conditions (Godfroy et al., 2024) may allow earlier detection of trees or stands that are affected by water stress and that have implemented strategies to regulate stomatal conductance.

5.4. Future research and management implications

Overall, these two opposing behaviors in the face of drought allow us to draw an analogy to Aesop's fable of the ant and the grasshopper. The upstream trees behave like the grasshopper: they do not sing all summer, but they do evapotranspire, reducing their leaf water content and water potential to the point where they may find themselves at high risk of cavitation. Meanwhile, the downstream trees behave more like the Ant, trying to limit their water use as much as possible to ensure long-term drought resistance. However, unlike the fable, even the behavior of the Ant (downstream trees) may affect tree survival in the long run. Upstream trees that fail to regulate transpiration and close stomata are at high risk of hydraulic failure, which is the primary cause of drought-induced mortality (McDowell, 2011). This risk can occur in the short term and prevents trees from recovering (Bréda et al., 2006; Martinez-Vilalta et al., 2019). While downstream trees, whose isohydric behavior reduces water loss, are less exposed to hydraulic failure, they are not risk-free. The reduction in transpiration and thus gas exchange also reduces carbon assimilation, which can lead to carbon starvation and mortality in the long term (McDowell et al., 2008).

The ability of white poplar to adapt to different climatic conditions, either through evolution or plasticity, highlights a capacity that has rarely been demonstrated on an intraspecific scale. These responses raise several questions about the ability of trees to adapt to climate change. Can upstream trees adopt a response behavior similar to that of the downstream trees at a pace and a scale that would allow them to withstand the increasing intensity and frequency of drought episodes? How long and to which point will the response strategy adopted by downstream trees be sufficient to cope with warmer and drier summers? Will their plastic behavior help them move on to new adaptive strategies once the risks associated with lower carbon assimilation will outweigh the benefits from reduced water loss? Similarly, given the high inter-individual variability and the fact that white poplar is a riparian species, we believe that it is essential to better characterize the local conditions in which each individual is located (Portela et al., 2023). A better understanding of the role of local conditions in the physiological responses of trees may subsequently allow us to promote targeted adaptation measures to increase the resilience of riparian forests to drought.

6. Conclusion

The role of riparian ecosystems is fundamental in the adaptation of other ecosystems to global change; therefore, understanding how to preserve and promote the resilience of these ecosystems to drought is imperative. Here, we show that white poplars along a hydroclimatic gradient have different responses and strategies to drought. We also show that understanding these differences requires the use of multiple methods and metrics to account for responses at different spatial and temporal scales. Our results suggest that white poplars have a high degree of physiological trait plasticity as a function of climatic conditions. However, further research is needed on the local factors that drive drought resistance in riparian trees, but there is also an urgent need to accurately measure tree responses to water stress at large scales. From a remote sensing perspective, we found that temperature is an accurate proxy of transpiration that can help establish stress conditions, while visible and near-infrared reflectance can help assess longer-term tree responses (such as leaf yellowing and biomass loss) to those stress conditions. In this regard, coupling data from the visible, near-infrared, and thermal infrared spectra shows promising results for working at large spatial scales to better characterize the response of riparian stands to water stress.

CRediT authorship contribution statement

Pierre Lochin: Writing – review & editing, Writing – original draft, Visualization, Methodology, Formal analysis, Data curation, Conceptualization. **Pauline Malherbe:** Writing – review & editing, Writing – original draft, Visualization, Formal analysis, Data curation, Conceptualization. **Baptiste Marteau:** Writing – review & editing, Methodology, Data curation, Conceptualization. **Julien Godfroy:** Writing – review & editing, Data curation. **Flavie Gerle:** Writing – review & editing, Data curation. **John Marshall:** Writing – review & editing. **Sara Puijalon:** Writing – review & editing. **Michael Bliss Singer:** Writing – review & editing, Funding acquisition. **John C. Stella:** Writing – review & editing, Funding acquisition. **Hervé Piégay:** Writing – review & editing, Funding acquisition, Conceptualization. **Antoine Vernay:** Writing – review & editing, Writing – original draft, Methodology, Funding acquisition, Data curation, Conceptualization.

Declaration of competing interest

The authors declare that they have no known competing financial interests or personal relationships that could have appeared to influence the work reported in this paper.

Data availability

Data will be made available on request.

Acknowledgements

This work was supported by the Labex DRIIHM French program “Investissements d'Avenir” (ANR-11-LABX-0010) of the Observatoire Hommes-Milieux Vallée du Rhône (OHM VR), managed by the ANR, and by the FR BioEnviS. The first author was also supported by the Graduate School H2O'Lyon (ANR-17-EURE-0018) of Université de Lyon (UdL), within the program “Investissements d'Avenir” operated by the French National Research Agency (ANR), by the National Science Foundation (EAR 1700517, EAR 1700555, and BCS 1660490), and by the U.S. Department of Defense's Strategic Environmental Research and Development Program-SERDP (RC18-1006). J.G. was supported by the Graduate School H2O'Lyon and by the Rhône-Méditerranée-Corse Water Agency. B.M. was supported by a grant from the France Relance national program.

We would like to thank the CEN Isère and the réserve naturelle du Haut-Rhône Français, especially Yves Prat-Mairet, Manon Bounous and Rémi Bogey, for their help in identifying sites and for their assistance in obtaining authorization to access the national nature reserves. We also thank Franck Toussaint ULM for the long-lasting and fruitful collaboration in conducting ultralight trike surveys.

Appendix A. Supplementary data

Supplementary data to this article can be found online at https://doi.org/10.1016/j.scitotenv.2024.175916.

References

Adler, P.B., Salguero-Gómez, R., Compagnoni, A., Hsu, J.S., Ray-Mukherjee, J., Mbeau-Ache, C., Franco, M., 2014. Functional traits explain variation in plant life history strategies. Proc. Natl. Acad. Sci. 111 (2), 740–745. https://doi.org/10.1073/pnas.1315179111.

Aguilar, C., Zinnert, J.C., Polo, M.J., Young, D.R., 2012. NDVI as an indicator for changes in water availability to woody vegetation. Ecol. Indic. 23, 290–300. https://doi.org/10.1016/j.ecolind.2012.04.008.

Allen, R.G., Pereira, L.S., Raes, D., Smith, M., et al., 1998. Crop evapotranspiration-guidelines for computing crop water requirements-FAO irrigation and drainage paper 56. Fao, Rome 300 (9), D05109.

Anderegg, W.R.L., Klein, T., Bartlett, M., Sack, L., Pellegrini, A.F.A., Choat, B., Jansen, S., 2016. Meta-analysis reveals that hydraulic traits explain cross-species patterns of drought-induced tree mortality across the globe. Proc. Natl. Acad. Sci. 113 (18), 5024–5029. https://doi.org/10.1073/pnas.1525678113.

Baker, K.V., Tai, X., Miller, M.L., Johnson, D.M., 2019. Six co-occurring conifer species in northern Idaho exhibit a continuum of hydraulic strategies during an extreme drought year. AoB PLANTS 11 (5), plz056. https://doi.org/10.1093/aobpla/plz056.

Bassman, J.H., Zwier, J.C., 1991. Gas exchange characteristics of Populus trichocarpa, Populus deltoides and Populus trichocarpa × P. deltoides clones. Tree Physiol. 8 (2), 145–159. https://doi.org/10.1093/treephys/8.2.145.

Bates, D., Maechler, M., Bolker, B., et al., 2012. Lme4: Linear Mixed-effects Models Using S4 Classes (R package version 0.999999-0. Vienna).

Beguería, S., Vicente-Serrano, S.M., Angulo-Martínez, M., 2010. A multiscalar global drought dataset: the SPEIBASE: A new gridded product for the analysis of drought variability and impacts. Bull. Am. Meteorol. Soc. 91 (10), 1351–1354.

Ben-Gal, A., Agam, N., Alchanatis, V., Cohen, Y., Yermiyahu, U., Zipori, I., Presnov, E., Sprintsin, M., Dag, A., 2009. Evaluating water stress in irrigated olives: correlation of soil water status, tree water status, and thermal imagery. Irrig. Sci. 27 (5), 367–376. https://doi.org/10.1007/s00271-009-0150-7.

Bennett, A.C., McDowell, N.G., Allen, C.D., Anderson-Teixeira, K.J., 2015. Larger trees suffer most during drought in forests worldwide. Nature Plants 1 (10), 10. https://doi.org/10.1038/nplants.2015.139.

Berni, J.A.J., Zarco-Tejada, P.J., Sepulcre-Cantó, G., Fereres, E., Villalobos, F., 2009. Mapping canopy conductance and CWSI in olive orchards using high resolution thermal remote sensing imagery. Remote Sens. Environ. 113 (11), 2380–2388. https://doi.org/10.1016/j.rse.2009.06.018.

Blake, T.J., Tschaplinski, T.J., Eastham, A., 1984. Stomatal control of water use efficiency in poplar clones and hybrids. Can. J. Bot. 62 (7), 1344–1351. https://doi.org/10.1139/b84-182.

Braatne, J.H., Rood, S.B., Heilman, P.E., 1996. Life history, ecology, and conservation of riparian cottonwoods in North America. Biology of Populus and Its Implications for Management and Conservation, Part I, 57–85.

Bravard, J.P., Gaydou, P., 2015. Historical development and integrated management of the Rhône River floodplain, from the Alps to the Camargue Delta, France. Geomorphic Approaches to Integrated Floodplain Management of Lowland Fluvial Systems in North America and Europe 289–320.

Bréda, N., Huc, R., Granier, A., Dreyer, E., 2006. Temperate forest trees and stands under severe drought: a review of ecophysiological responses, adaptation processes and long-term consequences. Ann. For. Sci. 63 (6), 625–644. https://doi.org/10.1051/forest:2006042.

BRLi, 2023. Étude de l'hydrologie du fleuve Rhône sous changement climatique.

Brooks, K.N., Folliott, P.F., Magner, J.A., 2012. Groundwater and groundwater–surface water exchange. In: Brooks, K.N., Folliott, P.F., Magner, J.A. (Eds.), Hydrology and the Management of Watersheds. https://doi.org/10.1002/9781118459751.ch7.

Capon, S.J., Chambers, L.E., Mac Nally, R., Naiman, R.J., Davies, P., Marshall, N., Pittock, J., Reid, M., Capon, T., Douglas, M., Catford, J., Baldwin, D.S., Stewardson, M., Roberts, J., Parsons, M., Williams, S.E., 2013. Riparian ecosystems in the 21st century: hotspots for climate change adaptation? Ecosystems 16 (3), 359–381. https://doi.org/10.1007/s10021-013-9656-1.

Choat, B., Brodribb, T.J., Brodersen, C.R., Duursma, R.A., López, R., Medlyn, B.E., 2018. Triggers of tree mortality under drought. Nature 558 (7711), 7711. https://doi.org/10.1038/s41586-018-0240-x.

Cornes, R.C., van der Schrier, G., van den Besselaar, E.J.M., Jones, P.D., 2018. An ensemble version of the E-OBS temperature and precipitation data sets. J. Geophys. Res. Atmos. 123 (17), 9391–9409. https://doi.org/10.1029/2017JD028200.

Crouchet, S.E., Jensen, J., Schwartz, B.F., Schwinning, S., 2019. Tree mortality after a hot drought: distinguishing density-dependent and -independent drivers and why it matters. Frontiers in Forests and Global Change 2. https://www.frontiersin.org/articles/10.3389/ffgc.2019.00021.

DeWoody, J., Trewin, H., Taylor, G., 2015. Genetic and morphological differentiation in Populus nigra L.: isolation by colonization or isolation by adaptation? Mol. Ecol. 24 (11), 2641–2655. https://doi.org/10.1111/mec.13192.

Dunlap, J.M., Stettler, R.F., 2001. Variation in leaf epidermal and stomatal traits of Populus trichocarpa from two transects across the Washington Cascades. Can. J. Bot. 79 (5), 528–536. https://doi.org/10.1139/b01-029.

Džubáková, K., Piégay, H., Riquier, J., Trizna, M., 2015. Multi-scale assessment of overflow-driven lateral connectivity in floodplain and backwater channels using LiDAR imagery. Hydrol. Process. 29 (10), 2315–2330. https://doi.org/10.1002/hyp.10361.

Fichot, R., Lefebvre, M., Pégard, M., Chassagnaud, D., Bliard, M., Ferdinand, J., Laurans, F., Thiec, D.L., Deveau, A., Stella, J.C., Rozenberg, P., Villar, M., 2024. Distinct trait syndromes and plasticity maintain similar performance between seedlings populations of the riparian tree species Populus nigra L. Environ. Exp. Bot. 218, 105598 https://doi.org/10.1016/j.envexpbot.2023.105598.

Friedman, J.M., Eurich, A.M., Auble, G.T., Scott, M.L., Shafroth, P.B., Gibson, P.P., 2022. Response of riparian vegetation to short- and long-term hydrologic variation. Ecol. Appl. 32 (8), e2689 https://doi.org/10.1002/eap.2689.

Fu, X., Meinzer, F.C., 2019. Metrics and proxies for stringency of regulation of plant water status (iso/anisohydry): a global data set reveals coordination and trade-offs among water transport traits. Tree Physiol. 39 (1), 122–134. https://doi.org/10.1093/treephys/tpy087.

Fuchs, M., 1990. Infrared measurement of canopy temperature and detection of plant water stress. Theor. Appl. Climatol. 42 (4), 253–261. https://doi.org/10.1007/BF00865986.

Fuchs, S., Leuschner, C., Mathias Link, R., Schuldt, B., 2021. Hydraulic variability of three temperate broadleaf tree species along a water availability gradient in central Europe. New Phytol. 231 (4), 1387–1400. https://doi.org/10.1111/nph.17448.

Garavillon-Tournayre, M., Gousset-Dupont, A., Gautier, F., Benoit, P., Conchon, P., Souchal, R., Lopez, D., Petel, G., Venisse, J.-S., Bastien, C., Label, P., Fumanal, B., 2018. Integrated drought responses of black poplar: how important is phenotypic plasticity? Physiol. Plant. 163 (1), 30–44. https://doi.org/10.1111/ppl.12646.

Gazol, A., Camarero, J.J., Sangüesa-Barreda, G., Serra-Maluquer, X., Sánchez-Salguero, R., Coll, L., Casals, P., 2020. Tree species are differently impacted by cumulative drought stress and present higher growth synchrony in dry places. Frontiers in Forests and Global Change 3. https://www.frontiersin.org/articles/10.3389/ffgc.2020.573346.

Gebre, G.M., Kuhns, M.R., 1993. Effects of water stress preconditioning on gas exchange and water relations of Populusdeltoides clones. Can. J. For. Res. 23 (7), 1291–1297. https://doi.org/10.1139/x93-165.

Gerle, F., Malherbe, P., Boisselet, C., Lafleuriel, D., Godfroy, J., Lochin, P., Marteau, B., Piegay, H., Puijalon, S., Vernay, A.. Intrinsic water use efficiency estimate: an isotopic method. https://www.protocols.io/view/intrinsic-water-use-efficiency-estimate-an-isotopi-c4fhytj6.

Godfroy, J., Malherbe, P., Gerle, F., Marteau, B., Lochin, P., Puijalon, S., Lejot, J., Vernay, A., Piégay, H., 2024. Can Multi-scale Thermal Infrared Imaging Help Validate and Monitor Water Stress in Alluvial Forests?.

Gomes Marques, I., Campelo, F., Rivaes, R., Albuquerque, A., Ferreira, M.T., Rodríguez-González, P.M., 2018. Tree rings reveal long-term changes in growth resilience in Southern European riparian forests. Dendrochronologia 52, 167–176. https://doi.org/10.1016/j.dendro.2018.10.009.

Gonzalez-Dugo, V., Zarco-Tejada, P., Berni, J.A.J., Suárez, L., Goldhamer, D., Fereres, E., 2012. Almond tree canopy temperature reveals intra-crown variability that is water stress-dependent. Agric. For. Meteorol. 154–155, 156–165. https://doi.org/10.1016/j.agrformet.2011.11.004.

González-Muñoz, N., Sterck, F., Torres-Ruiz, J.M., Petit, G., Cochard, H., Arx, G. von, Lintunen, A., Caldeira, M.C., Capdeville, G., Copini, P., Gebauer, R., Grönlund, L., Hölttä, T., Lobo-do-Vale, R., Peltoniemi, M., Stritih, A., Urban, J., Delzon, S., 2018. Quantifying in situ phenotypic variability in the hydraulic properties of four tree species across their distribution range in Europe. PloS One 13 (5), e0196075. https://doi.org/10.1371/journal.pone.0196075.

Gorelick, N., Hancher, M., Dixon, M., Ilyushchenko, S., Thau, D., Moore, R., 2017. Google Earth Engine: planetary-scale geospatial analysis for everyone. Remote Sens. Environ. 202, 18–27. https://doi.org/10.1016/j.rse.2017.06.031.

Herbette, S., Wortemann, R., Awad, H., Huc, R., Cochard, H., Barigah, T.S., 2010. Insights into xylem vulnerability to cavitation in Fagus sylvatica L.: phenotypic and environmental sources of variability. Tree Physiol. 30 (11), 1448–1455. https://doi.org/10.1093/treephys/tpq079.

Hernández-Clemente, R., Hornero, A., Mottus, M., Penuelas, J., González-Dugo, V., Jiménez, J.C., Suárez, L., Alonso, L., Zarco-Tejada, P.J., 2019. Early diagnosis of vegetation health from high-resolution hyperspectral and thermal imagery: lessons learned from empirical relationships and radiative transfer modelling. Curr. For. Rep. 5 (3), 169–183. https://doi.org/10.1007/s40725-019-00096-1.

Hydrofis-Brli, 2015. Gestion de la nappe alluviale du Rhône court-circuité de Péage-de-Roussillon.

Janssen, P., Stella, J.C., Piégay, H., Räpple, B., Pont, B., Faton, J.-M., Cornelissen, J.H.C., Evette, A., 2020. Divergence of riparian forest composition and functional traits from natural succession along a degraded river with multiple stressor legacies. Sci. Total Environ. 721, 137730 https://doi.org/10.1016/j.scitotenv.2020.137730.

Jones, H.G., Archer, N., Rotenberg, E., Casa, R., 2003. Radiation measurement for plant ecophysiology. J. Exp. Bot. 54 (384), 879–889. https://doi.org/10.1093/jxb/erg116.

Jones, H.G., Serraj, R., Loveys, B.R., Xiong, L., Wheaton, A., Price, A.H., 2009. Thermal infrared imaging of crop canopies for the remote diagnosis and quantification of plant responses to water stress in the field. Funct. Plant Biol. 36 (11), 978–989. https://doi.org/10.1071/FP09123.

Jones, H.G., Hutchinson, P.A., May, T., Jamali, H., Deery, D.M., 2018. A practical method using a network of fixed infrared sensors for estimating crop canopy conductance and evaporation rate. Biosyst. Eng. 165, 59–69. https://doi.org/10.1016/j.biosystemseng.2017.09.012.

Kang, J., Shen, H., Zhang, S., Xu, L., Tang, Z., Tang, Y., Fang, J., 2024. Contrasting growth responses to drought in three tree species widely distributed in northern China. Sci. Total Environ. 908, 168331 https://doi.org/10.1016/j.scitotenv.2023.168331.

Keller, S.R., Soolanayakanahally, R.Y., Guy, R.D., Silim, S.N., Olson, M.S., Tiffin, P., 2011. Climate-driven local adaptation of ecophysiology and phenology in balsam poplar, Populus balsamifera L. (Salicaceae). Am. J. Bot. 98 (1), 99–108. https://doi.org/10.3732/ajb.1000317.

Kelly, R., Healy, K., Anand, M., Baudraz, M.E.A., Bahn, M., Cerabolini, B.E.L., Cornelissen, J.H.C., Dwyer, J.M., Jackson, A.L., Kattge, J., Niinemets, Ü., Penuelas, J., Pierce, S., Salguero-Gómez, R., Buckley, Y.M., 2021. Climatic and evolutionary contexts are required to infer plant life history strategies from functional traits at a global scale. Ecol. Lett. 24 (5), 970–983. https://doi.org/10.1111/ele.13704.

Kibler, C.L., Schmidt, E.C., Roberts, D.A., Stella, J.C., Kui, L., Lambert, A.M., Singer, M.B., 2021. A brown wave of riparian woodland mortality following groundwater declines during the 2012–2019 California drought. Environ. Res. Lett. 16 (8), 084030 https://doi.org/10.1088/1748-9326/ac1377.

Kibler, C.L., Trugman, A.T., Roberts, D.A., Still, C.J., Scott, R.L., Caylor, K.K., Stella, J.C., Singer, M.B., 2023. Evapotranspiration regulates leaf temperature and respiration in dryland vegetation. Agric. For. Meteorol. 339, 109560 https://doi.org/10.1016/j.agrformet.2023.109560.

Labroche, A., Pont, B., Prat-Mairet, Y., 2017. Réponse des communautés amphibies et terrestres à l'augmentation du débit réservé sur le vieux Rhône de Péage de Roussillon. CEN Isère – Antenne Platière. Coll.

Lamouroux, N., Gore, J.A., Lepori, F., Statzner, B., 2015. The ecological restoration of large rivers needs science-based, predictive tools meeting public expectations: an overview of the Rhône project. Freshw. Biol. 60 (6), 1069–1084. https://doi.org/10.1111/fwb.12553.

Lapidot, O., Ignat, T., Rud, R., Rog, I., Alchanatis, V., Klein, T., 2019. Use of thermal imaging to detect evaporative cooling in coniferous and broadleaved tree species of the Mediterranean maquis. Agric. For. Meteorol. 271, 285–294. https://doi.org/10.1016/j.agrformet.2019.02.014.

Larchevêque, M., Maurel, M., Desrochers, A., Larocque, G.R., 2011. How does drought tolerance compare between two improved hybrids of balsam poplar and an unimproved native species? Tree Physiol. 31 (3), 240–249. https://doi.org/10.1093/treephys/tpr011.

Larter, M., Pfautsch, S., Domec, J.-C., Trueba, S., Nagalingum, N., Delzon, S., 2017. Aridity drove the evolution of extreme embolism resistance and the radiation of conifer genus Callitris. New Phytol. 215 (1), 97–112. https://doi.org/10.1111/nph.14545.

Le, T.S., Harper, R., Dell, B., 2023. Application of remote sensing in detecting and monitoring water stress in forests. Remote Sens. (Basel) 15 (13), 13. https://doi.org/10.3390/rs15133360.

Lenth, R.V., 2023. emmeans: Estimated Marginal Means, aka Least-squares Means [Manual]. https://CRAN.R-project.org/package=emmeans.

Li, J., Roy, D.P., 2017. A global analysis of sentinel-2A, sentinel-2B and Landsat-8 data revisit intervals and implications for terrestrial monitoring. Remote Sens. (Basel) 9 (9), 9. https://doi.org/10.3390/rs9090902.

Lisar, Motafakkerazad, R., M., M., M. Rahm, I.M., 2012. Water stress in plants: causes, effects and responses. In: Md, I., Rahman, M. (Eds.), Water Stress. InTech. https://doi.org/10.5772/39363.

Lochin, P., Piégay, H., Stella, J. C., Kelly, C., Vaudor, L., & Singer, M. B. (in review). Drivers of Spatiotemporal Patterns of Riparian Forest NDVI Along a Hydroclimatic Gradient.

Ma, Zhang, B., Jia, L., Huang, H., 2020. Conditional distribution selection for SPEI-daily and its revealed meteorological drought characteristics in China from 1961 to 2017. Atmos. Res. 246, 105108 https://doi.org/10.1016/j.atmosres.2020.105108.

Ma, Li, Y., Liu, F., Feng, H., Biswas, A., Zhang, Q., 2023. SPEI and multi-threshold run theory based drought analysis using multi-source products in China. J. Hydrol. 616, 128737 https://doi.org/10.1016/j.jhydrol.2022.128737.

Maherali, H., Pockman, W.T., Jackson, R.B., 2004. Adaptive variation in the vulnerability of woody plants to xylem cavitation. Ecology 85 (8), 2184–2199. https://doi.org/10.1890/02-0538.

Marron, N., Delay, D., Petit, J.-M., Dreyer, E., Kahlem, G., Delmotte, F.M., Brignolas, F., 2002. Physiological traits of two Populus × euramericana clones, Luisa Avanzo and Dorskamp, during a water stress and re-watering cycle. Tree Physiol. 22 (12), 849–858. https://doi.org/10.1093/treephys/22.12.849.

Martínez-Vilalta, J., Garcia-Forner, N., 2017. Water potential regulation, stomatal behaviour and hydraulic transport under drought: deconstructing the iso/anisohydric concept. Plant Cell Environ. 40 (6), 962–976. https://doi.org/10.1111/pce.12846.

Martinez-Vilalta, J., Anderegg, W.R.L., Sapes, G., Sala, A., 2019. Greater focus on water pools may improve our ability to understand and anticipate drought-induced mortality in plants. New Phytol. 223 (1), 22–32. https://doi.org/10.1111/nph.15644.

Martin-StPaul, N.K., Limousin, J.-M., Vogt-Schilb, H., Rodríguez-Calcerrada, J., Rambal, S., Longepierre, D., Misson, L., 2013. The temporal response to drought in a Mediterranean evergreen tree: comparing a regional precipitation gradient and a throughfall exclusion experiment. Glob. Chang. Biol. 19 (8), 2413–2426. https://doi.org/10.1111/gcb.12215.

Marusig, D., Petruzzellis, F., Tomasella, M., Napolitano, R., Altobelli, A., Nardini, A., 2020. Correlation of field-measured and remotely sensed plant water status as a tool to monitor the risk of drought-induced forest decline. Forests 11 (1), 1. https://doi.org/10.3390/f11010077.

McDowell, N.G., 2011. Mechanisms linking drought, hydraulics, carbon metabolism, and vegetation mortality. Plant Physiol. 155 (3), 1051–1059. https://doi.org/10.1104/pp.110.170704.

McDowell, N.G., Pockman, W.T., Allen, C.D., Breshears, D.D., Cobb, N., Kolb, T., Plaut, J., Sperry, J., West, A., Williams, D.G., Yepez, E.A., 2008. Mechanisms of plant survival and mortality during drought: why do some plants survive while others succumb to drought? New Phytol. 178 (4), 719–739. https://doi.org/10.1111/j.1469-8137.2008.02436.x.

McDowell, N.G., Sapes, G., Pivovaroff, A., Adams, H.D., Allen, C.D., Anderegg, W.R.L., Arend, M., Breshears, D.D., Brodribb, T., Choat, B., Cochard, H., De Cáceres, M., De Kauwe, M.G., Grossiord, C., Hammond, W.M., Hartmann, H., Hoch, G., Kahmen, A., Klein, T., Xu, C., 2022. Mechanisms of woody-plant mortality under rising drought, CO2 and vapour pressure deficit. Nature Reviews Earth & Environment 3 (5), 5. https://doi.org/10.1038/s43017-022-00272-1.

Nie, C., Huang, Y., Zhang, S., Yang, Y., Zhou, S., Lin, C., Wang, G., 2021. Effects of soil water content on forest ecosystem water use efficiency through changes in transpiration/evapotranspiration ratio. Agric. For. Meteorol. 308–309, 108605 https://doi.org/10.1016/j.agrformet.2021.108605.

Nolan, R.H., Gauthey, A., Losso, A., Medlyn, B.E., Smith, R., Chhajed, S.S., Fuller, K., Song, M., Li, X., Beaumont, L.J., Boer, M.M., Wright, I.J., Choat, B., 2021. Hydraulic failure and tree size linked with canopy die-back in eucalypt forest during extreme drought. New Phytol. 230 (4), 1354–1365. https://doi.org/10.1111/nph.17298.

Olivier, J.-M., Carrel, G., Lamouroux, N., Dole-Olivier, M.-J., Malard, F., Bravard, J.P., Piégay, H., Castella, E., Barthélemy, C., 2022. Chapter 7—the Rhône River basin. In: Tockner, K., Zarfl, C., Robinson, C.T. (Eds.), Rivers of Europe, Second edition. Elsevier, pp. 391–451. https://doi.org/10.1016/B978-0-08-102612-0.00007-9.

Pace, G., Gutiérrez-Cánovas, C., Henriques, R., Boeing, F., Cássio, F., Pascoal, C., 2021. Remote sensing depicts riparian vegetation responses to water stress in a humid Atlantic region. Sci. Total Environ. 772, 145526 https://doi.org/10.1016/j.scitotenv.2021.145526.

Palmer, M.a., Reidy Liermann, C.A., Nilsson, C., Flörke, M., Alcamo, J., Lake, P.S., Bond, N., 2008. Climate change and the world's river basins: anticipating management options. Front. Ecol. Environ. 6 (2), 81–89. https://doi.org/10.1890/060148.

Pearce, D.W., Millard, S., Bray, D.F., Rood, S.B., 2006. Stomatal characteristics of riparian poplar species in a semi-arid environment. Tree Physiol. 26 (2), 211–218. https://doi.org/10.1093/treephys/26.2.211.

Pérez-Harguindeguy, N., Díaz, S., Garnier, E., Lavorel, S., Poorter, H., Jaureguiberry, P., Bret-Harte, M.S., Cornwell, W.K., Craine, J.M., Gurvich, D.E., Urcelay, C., Veneklaas, E.J., Reich, P.B., Poorter, L., Wright, I.J., Ray, P., Enrico, L., Pausas, J.G., Vos, A.C. de, Cornelissen, J.H.C., 2016. Corrigendum to: new handbook for standardised measurement of plant functional traits worldwide. Aust. J. Bot. 64 (8), 715–716. https://doi.org/10.1071/bt12225_co.

Perry, L., Andersen, D., Reynolds, L., Nelson, S., Shafroth, P., 2012. Vulnerability of riparian ecosystems to elevated CO2 and climate change in arid and semiarid western North America. Glob. Chang. Biol. 18 https://doi.org/10.1111/j.1365-2486.2011.02588.x.

Peters, J.M.R., López, R., Nolf, M., Hutley, L.B., Wardlaw, T., Cernusak, L.A., Choat, B., 2021. Living on the edge: a continental-scale assessment of forest vulnerability to drought. Glob. Chang. Biol. 27 (15), 3620–3641. https://doi.org/10.1111/gcb.15641.

Pettit, N., Froend, R., 2018. How important is groundwater availability and stream perenniality to riparian and floodplain tree growth? Hydrol. Process. 32 https://doi.org/10.1002/hyp.11510.

Pohl, F., Rakovec, O., Rebmann, C., Hildebrandt, A., Boeing, F., Hermanns, F., Attinger, S., Samaniego, L., Kumar, R., 2023. Long-term daily hydrometeorological drought indices, soil moisture, and evapotranspiration for ICOS sites. Scientific Data 10 (1), 1. https://doi.org/10.1038/s41597-023-02192-1.

Portela, A.P., Gonçalves, J.F., Durance, I., Vieira, C., Honrado, J., 2023. Riparian forest response to extreme drought is influenced by climatic context and canopy structure. Sci. Total Environ. 881, 163128 https://doi.org/10.1016/j.scitotenv.2023.163128.

R Core Team, 2022. R: A Language and Environment for Statistical Computing. R Foundation for Statistical Computing, Vienna, Austria [Computer software]. https://www.R-project.org/.

Räpple, B., 2018. Sedimentation Patterns and Riparian Vegetation Characteristics in Novel Ecosystems on the Rhône River, France: A Comparative Approach to Identify Drivers and Evaluate Ecological Potentials (These de doctorat, Lyon). https://www.theses.fr/2018LYSEN006.

Reichstein, M., Bahn, M., Ciais, P., Frank, D., Mahecha, M.D., Seneviratne, S.I., Zscheischler, J., Beer, C., Buchmann, N., Frank, D.C., Papale, D., Rammig, A., Smith, P., Thonicke, K., van der Velde, M., Vicca, S., Walz, A., Wattenbach, M., 2013. Climate extremes and the carbon cycle. Nature 500 (7462), 7462. https://doi.org/10.1038/nature12350.

Rivaes, R., Rodríguez-González, P.M., Albuquerque, A., Pinheiro, A.N., Egger, G., Ferreira, M.T., 2013. Riparian vegetation responses to altered flow regimes driven by climate change in Mediterranean rivers. Ecohydrology 6 (3), 413–424. https://doi.org/10.1002/eco.1287.

Rohde, Stella, J.C., Roberts, D.A., Singer, M.B., 2021. Groundwater dependence of riparian woodlands and the disrupting effect of anthropogenically altered streamflow. Proc. Natl. Acad. Sci. 118 (25), e2026453118 https://doi.org/10.1073/pnas.2026453118.

Rood, S.B., Braatne, J.H., Hughes, F.M.R., 2003. Ecophysiology of riparian cottonwoods: stream flow dependency, water relations and restoration†. Tree Physiol. 23 (16), 1113–1124. https://doi.org/10.1093/treephys/23.16.1113.

Rood, S.B., Bigelow, S.G., Hall, A.A., 2011. Root architecture of riparian trees: river cut-banks provide natural hydraulic excavation, revealing that cottonwoods are facultative phreatophytes. Trees 25 (5), 907–917. https://doi.org/10.1007/s00468-011-0565-7.

Rosas, T., Mencuccini, M., Barba, J., Cochard, H., Saura-Mas, S., Martínez-Vilalta, J., 2019. Adjustments and coordination of hydraulic, leaf and stem traits along a water availability gradient. New Phytol. 223 (2), 632–646. https://doi.org/10.1111/nph.15684.

Rouse, J.W., Haas, R.H., Schell, J.A., Deering, D.W., et al., 1974. Monitoring vegetation systems in the Great Plains with ERTS. NASA Spec. Publ 351 (1), 309.

Ruehr, N.K., Gast, A., Weber, C., Daub, B., Arneth, A., 2016. Water availability as dominant control of heat stress responses in two contrasting tree species. Tree Physiol. 36 (2), 164–178. https://doi.org/10.1093/treephys/tpv102.

Sabathier, R., Singer, M.B., Stella, J.C., Roberts, D.A., Caylor, K.K., 2021. Vegetation responses to climatic and geologic controls on water availability in southeastern Arizona. Environ. Res. Lett. 16 (6), 064029 https://doi.org/10.1088/1748-9326/abfe8c.

Salazar Zarzosa, P., Diaz Herraiz, A., Olmo, M., Ruiz-Benito, P., Barrón, V., Bastias, C.C., de la Riva, E.G., Villar, R., 2021. Linking functional traits with tree growth and forest productivity in Quercus ilex forests along a climatic gradient. Sci. Total Environ. 786, 147468 https://doi.org/10.1016/j.scitotenv.2021.147468.

Sánchez-Pérez, J.M., Lucot, E., Bariac, T., Trémolières, M., 2008. Water uptake by trees in a riparian hardwood forest (Rhine floodplain, France). Hydrol. Process. 22 (3), 366–375. https://doi.org/10.1002/hyp.6604.

Sargeant, C.I., Singer, M.B., 2021. Local and non-local controls on seasonal variations in water availability and use by riparian trees along a hydroclimatic gradient, 16 (8), 084018. https://doi.org/10.1088/1748-9326/ac1294.

Sauquet, E., Richard, B., Devers, A., Prudhomme, C., 2019. Water restrictions under climate change: a Rhône–Mediterranean perspective combining bottom-up and top-down approaches. Hydrol. Earth Syst. Sci. 23 (9), 3683–3710. https://doi.org/10.5194/hess-23-3683-2019.

Scholander, P.F., Bradstreet, E.D., Hemmingsen, E.A., Hammel, H.T., 1965. Sap pressure in vascular plants. Science 148 (3668), 339–346. https://doi.org/10.1126/science.148.3668.339.

Schuldt, B., Knutzen, F., Delzon, S., Jansen, S., Müller-Haubold, H., Burlett, R., Clough, Y., Leuschner, C., 2016. How adaptable is the hydraulic system of European beech in the face of climate change-related precipitation reduction? New Phytol. 210 (2), 443–458. https://doi.org/10.1111/nph.13798.

Singer, M.B., Stella, J.C., Dufour, S., Piégay, H., Wilson, R.J.S., Johnstone, L., 2013. Contrasting water-uptake and growth responses to drought in co-occurring riparian tree species. Ecohydrology 6 (3), 402–412. https://doi.org/10.1002/eco.1283.

Singer, M.B., Sargeant, C.I., Piégay, H., Riquier, J., Wilson, R.J.S., Evans, C.M., 2014. Floodplain ecohydrology: climatic, anthropogenic, and local physical controls on partitioning of water sources to riparian trees. Water Resour. Res. 50 (5), 4490–4513. https://doi.org/10.1002/2014WR015581.

Slette, I.J., Post, A.K., Awad, M., Even, T., Punzalan, A., Williams, S., Smith, M.D., Knapp, A.K., 2019. How ecologists define drought, and why we should do better. Glob. Chang. Biol. 25 (10), 3193–3200. https://doi.org/10.1111/gcb.14747.

Smart, R.E., Bingham, G.E., 1974. Rapid estimates of relative water content. Plant Physiol. 53 (2), 258–260. https://doi.org/10.1104/pp.53.2.258.

Stojnić, S., Suchocka, M., Benito-Garzón, M., Torres-Ruiz, J.M., Cochard, H., Bolte, A., Cocozza, C., Cvjetković, B., de Luis, M., Martinez-Vilalta, J., Ræbild, A., Tognetti, R., Delzon, S., 2018. Variation in xylem vulnerability to embolism in European beech from geographically marginal populations. Tree Physiol. 38 (2), 173–185. https://doi.org/10.1093/treephys/tpx128.

Street, N.R., Skogström, O., Sjödin, A., Tucker, J., Rodríguez-Acosta, M., Nilsson, P., Jansson, S., Taylor, G., 2006. The genetics and genomics of the drought response in Populus. Plant J. 48 (3), 321–341. https://doi.org/10.1111/j.1365-313X.2006.02864.x.

Stromberg, J.C., Tiller, R., Richter, B., 1996. Effects of groundwater decline on riparian vegetation of semiarid regions: the San Pedro, Arizona. Ecological Applications 6 (1), 113–131. https://doi.org/10.2307/2269558.

Sturm, J., Santos, M.J., Schmid, B., Damm, A., 2022. Satellite data reveal differential responses of Swiss forests to unprecedented 2018 drought. Glob. Chang. Biol. 28 (9), 2956–2978. https://doi.org/10.1111/gcb.16136.

Szatniewska, J., Zavadilova, I., Nezval, O., Krejza, J., Petrik, P., Čater, M., Stojanović, M., 2022. Species-specific growth and transpiration response to changing environmental conditions in floodplain forest. For. Ecol. Manage. 516, 120248 https://doi.org/10.1016/j.foreco.2022.120248.

Tardieu, F., Simonneau, T., 1998. Variability among species of stomatal control under fluctuating soil water status and evaporative demand: modelling isohydric and anisohydric behaviours. J. Exp. Bot. 49, 419–432.

Tardieu, F., Tuberosa, R., 2010. Dissection and modelling of abiotic stress tolerance in plants. Curr. Opin. Plant Biol. 13 (2), 206–212. https://doi.org/10.1016/j.pbi.2009.12.012.

Taylor, C.J., Alley, W.M., 2001. Ground-water-level Monitoring and the Importance of Long-term water-level Data, vol. 1217. US Geological Survey, Denver, CO, USA.

Théroux-Rancourt, G., Éthier, G., Pepin, S., 2014. Threshold response of mesophyll CO2 conductance to leaf hydraulics in highly transpiring hybrid poplar clones exposed to soil drying. J. Exp. Bot. 65 (2), 741–753.

Vázquez-Tarrío, D., Tal, M., Camenen, B., Piégay, H., 2019. Effects of continuous embankments and successive run-of-the-river dams on bedload transport capacities along the Rhône River, France. Sci. Total Environ. 658, 1375–1389. https://doi.org/10.1016/j.scitotenv.2018.12.109.

Vernay, A., Tian, X., Chi, J., Linder, S., Mäkelä, A., Oren, R., Peichl, M., Stangl, Z.R., Tor-Ngern, P., Marshall, J.D., 2020. Estimating canopy gross primary production by combining phloem stable isotopes with canopy and mesophyll conductances. Plant Cell Environ. 43 (9), 2124–2142. https://doi.org/10.1111/pce.13835.

Vernay, A., Hasselquist, N., Leppä, K., Klosterhalfen, A., Gutierrez Lopez, J., Stangl, Z.R., Chi, J., Kozii, N., Marshall, J.D., 2024. Partitioning gross primary production of a boreal forest among species and strata: a multi-method approach. Agric. For. Meteorol. 345, 109857 https://doi.org/10.1016/j.agrformet.2023.109857.

Vicente-Serrano, S.M., Beguería, S., López-Moreno, J.I., 2010. A multiscalar drought index sensitive to global warming: the standardized precipitation evapotranspiration index. J. Climate 23 (7), 1696–1718. https://doi.org/10.1175/2009JCLI2909.1.

Viger, M., Smith, H.K., Cohen, D., Dewoody, J., Trewin, H., Steenackers, M., Bastien, C., Taylor, G., 2016. Adaptive mechanisms and genomic plasticity for drought tolerance identified in European black poplar (Populus nigra L.). Tree Physiol. 36 (7), 909–928. https://doi.org/10.1093/treephys/tpw017.

Wang, Q., Wu, J., Lei, T., He, B., Wu, Z., Liu, M., Mo, X., Geng, G., Li, X., Zhou, H., Liu, D., 2014. Temporal-spatial characteristics of severe drought events and their impact on agriculture on a global scale. Quat. Int. 349, 10–21. https://doi.org/10.1016/j.quaint.2014.06.021.

Warter, M.M., Singer, M.B., Cuthbert, M.O., Roberts, D., Caylor, K.K., Sabathier, R., Stella, J., 2023. Modeling seasonal vegetation phenology from hydroclimatic drivers for contrasting plant functional groups within drylands of the Southwestern USA. Environmental Research: Ecology 2 (2), 025001. https://doi.org/10.1088/2752-664X/acb9a0.

Weiwei, L.U., Xinxiao, Y.U., Guodong, J.I.A., Hanzhi, L.I., Ziqiang, L.I.U., 2018. Responses of intrinsic water-use efficiency and tree growth to climate change in semi-arid areas of North China. Sci. Rep. 8 (1), 1 https://doi.org/10.1038/s41598-017-18694-z.

Williams, Stella, J.C., Voelker, S.L., Lambert, A.M., Pelletier, L.M., Drake, J.E., Friedman, J.M., Roberts, D.A., Singer, M.B., 2022. Local groundwater decline exacerbates response of dryland riparian woodlands to climatic drought. Glob. Chang. Biol. 28 (22), 6771–6788. https://doi.org/10.1111/gcb.16376.

Williams, Stella, J. C., Singer, M. B., Lambert, A. M., Voelker, S. L., Drake, J. E., Friedman, J. M., Pelletier, L. M., Kui, L., & Roberts, D. A. (in review). Seasonal and species-level water-use strategies and groundwater dependence in dryland riparian woodlands during extreme drought. Water Resources Research.

Yakir, D., Sternberg, L. da S.L., 2000. The use of stable isotopes to study ecosystem gas exchange. Oecologia 123 (3), 297–311. https://doi.org/10.1007/s004420051016.

Zhang, X., Ci, X., Hu, J., Bai, Y., Thornhill, A.H., Conran, J.G., Li, J., 2023. Riparian areas as a conservation priority under climate change. Sci. Total Environ. 858, 159879 https://doi.org/10.1016/j.scitotenv.2022.159879.

The Ant and the Grasshopper: contrasting responses and behaviors to water stress of riparian trees along a hydroclimatic gradient

Pierre Lochin[1]*, Pauline Malherbe[1], Baptiste Marteau[1,2], Julien Godfroy[1,3], Flavie Gerle[4], John Marshall[5,6,7], Sara Puijalon[4], Michael Bliss Singer[8,9,10], John C. Stella[11], Hervé Piégay[1], Antoine Vernay[4]

[1]ENS de Lyon, UMR 5600 Environnement Ville société, CNRS, Lyon, France

[2]LETG UMR 6554, Université Rennes 2, Rennes, France

[3]Univ. Grenoble Alpes, INRAE, LESSEM, F-38402 St-Martin d'Hères, France

[4]Université Claude Bernard Lyon 1, LEHNA UMR 5023, CNRS, ENTPE, F-69622, Villeurbanne, France

[5]Global Change Research Institute, Czech Academy of Sciences, Bělidla 4a, 603 00 Brno, Czech Republic

[6]Leibniz-Zentrum für Agrarlandschaftsforschung, 15374 Müncheberg, Germany

[7]Department of Geological Sciences, Gothenburg University, Gothenburg, Sweden

[8]Earth Research Institute, University of California, Santa Barbara, CA 93106, USA

[9]Water Research Institute, Cardiff University, Cardiff CF10 3AX, UK

[10]School of Earth and Environmental Sciences, Cardiff University, Cardiff CF10 3AT, UK

[11]Department of Sustainable Resources Management, State University of New York College of Environmental Science and Forestry, Syracuse, NY 13210, USA

*Corresponding author

Email: pierre.lochin@ens-lyon.fr

Supplemental information

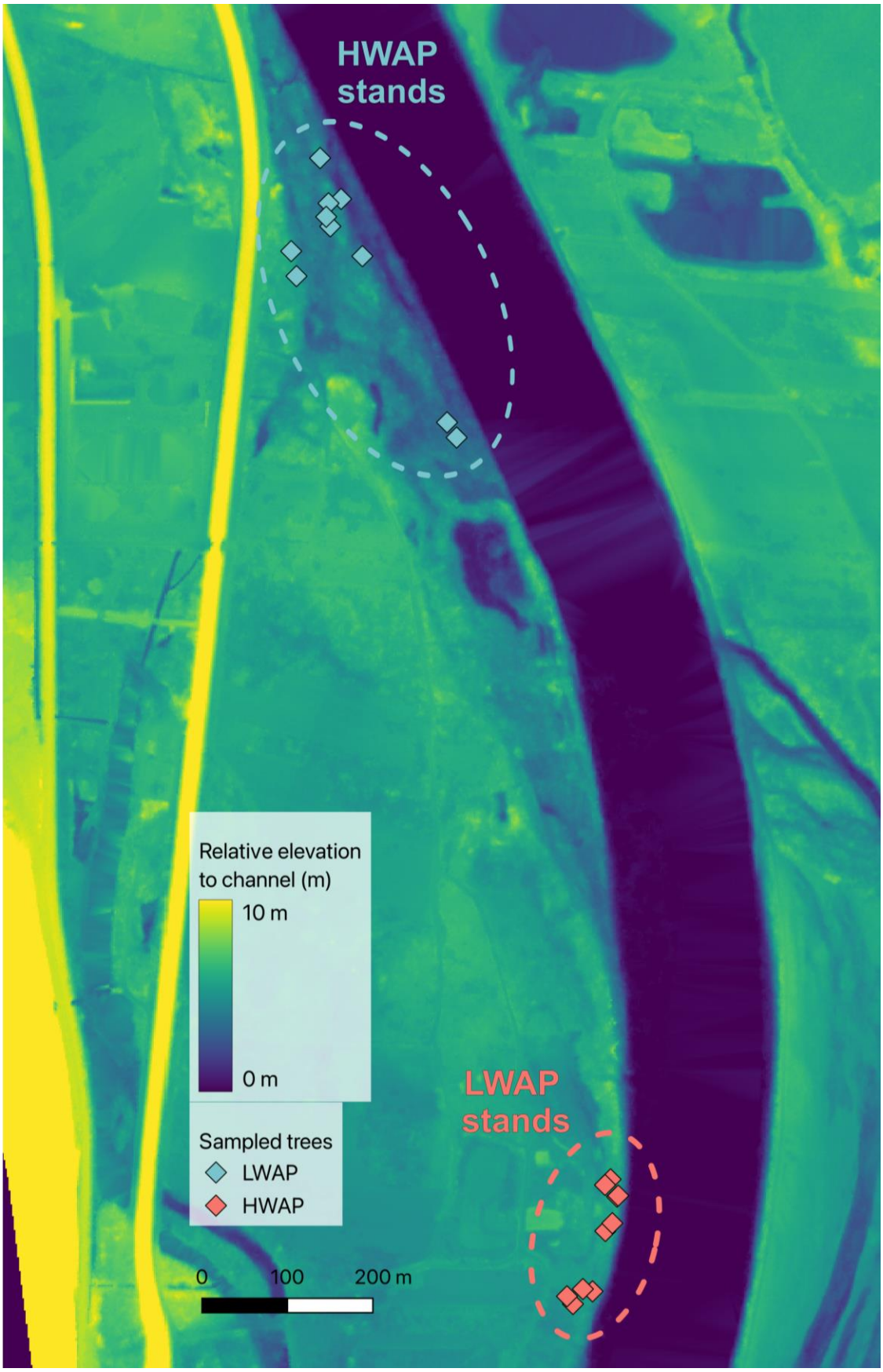

Fig. S 1 Relative elevation to the channel at the downstream site, with high water availability potential (HWAP, in blue) and low water availability potential (LWAP, in red) forest stands. Blue areas on the

map are low-elevation areas, while areas tending toward yellow are high-elevation areas relative to the channel

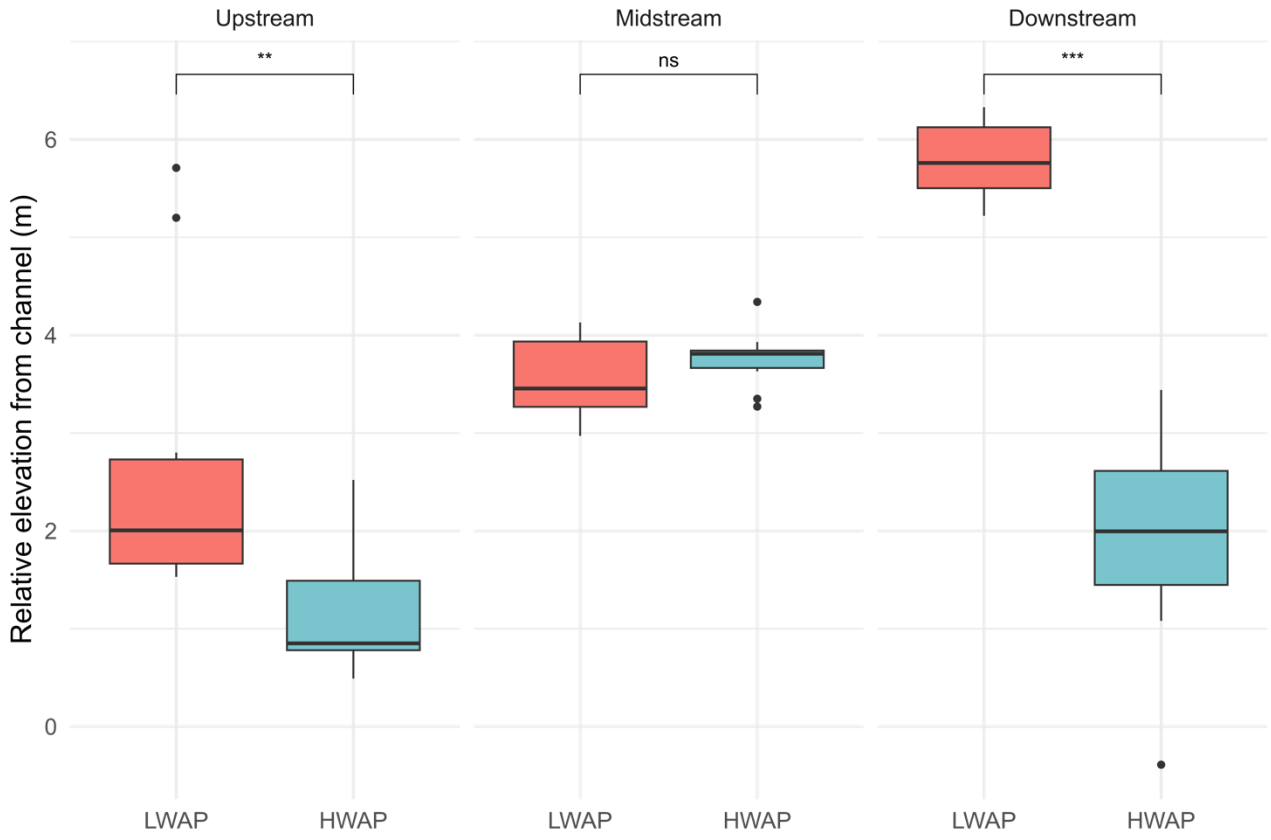

Fig. S 2 Tree relative elevation from the channel of each forest stand (Low Water Availability Potential and High WAP) and each of the three sites (upstream, midstream, downstream). * indicates that the difference between means is statistically significant according to the Wilcoxon test, with *** indicating $p < 0.001$, ** = $p < 0.01$, * = $p < 0.05$, and ns = $p > 0.05$.

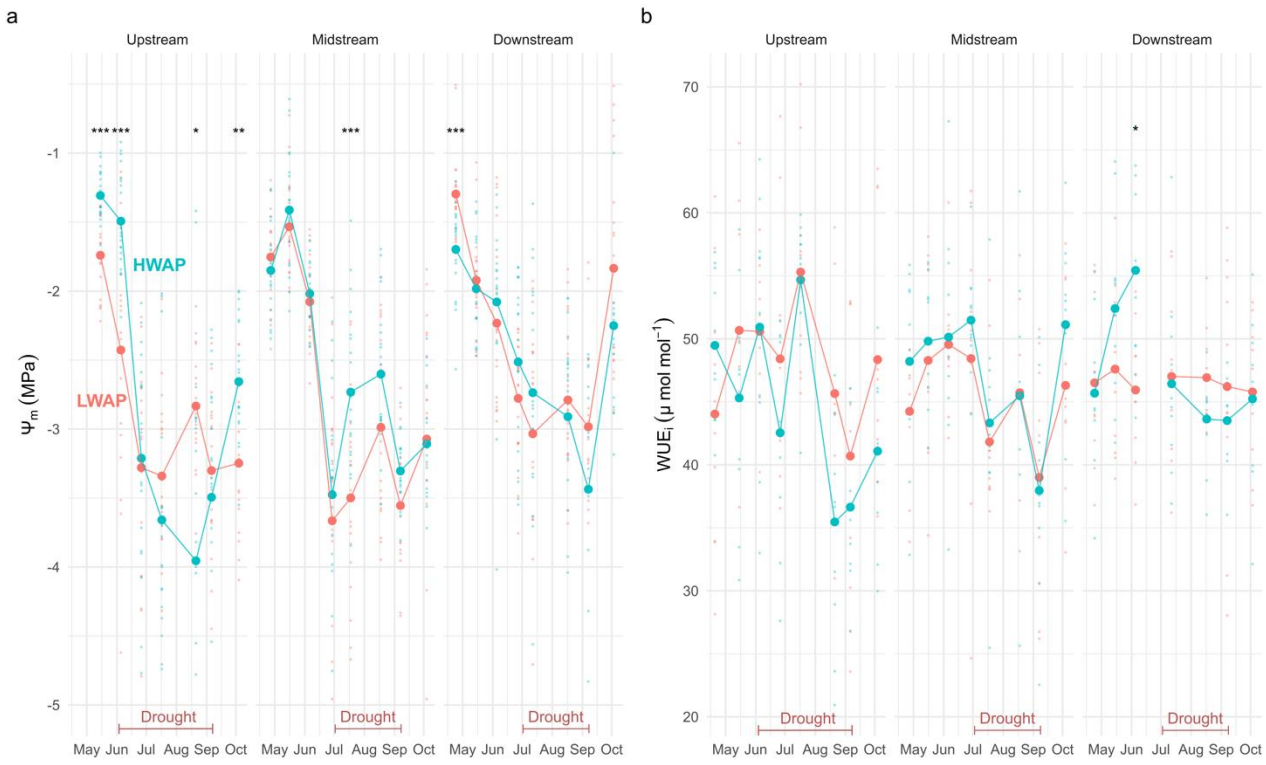

Fig. S 3 Dynamics of (a) minimum leaf water potential (Ψ_m) and (b) intrinsic water use efficiency (WUE_i) in each forest stand (Low Water Availability Potential, in red, High Water Availability Potential, in blue) and each sampling date. * indicates that the difference between means was statistically significant according to the Wilcoxon test, with *** indicating $p < 0.001$, ** = $p < 0.01$, * = $p < 0.05$, and ns = $p > 0.05$.

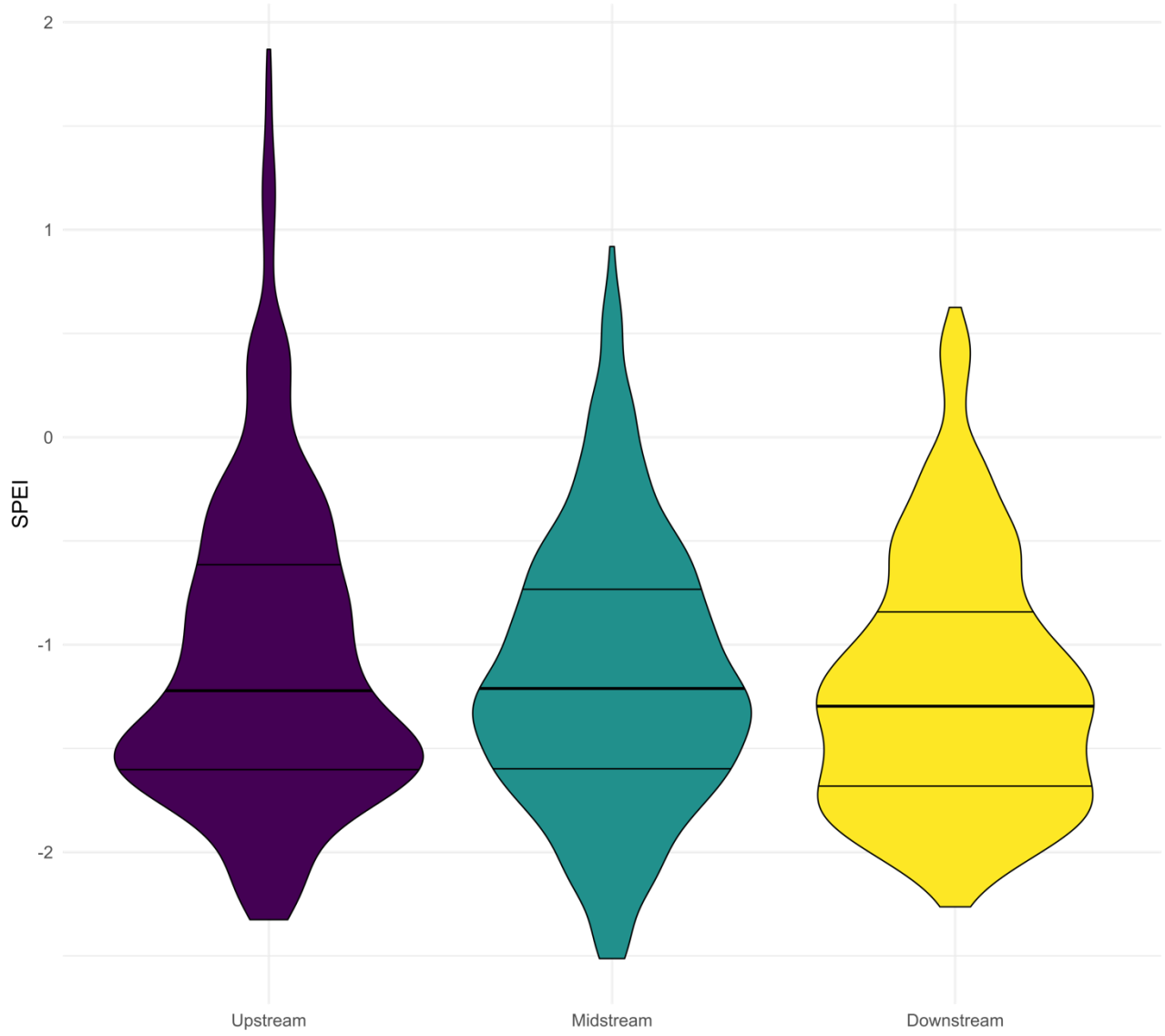

Fig. S 4 Distributions of 30-day SPEI values for the summer months (July-August) between 1995-2023.

Site	Forest stand	Tree diameter range (cm)	Mean diameter and standard deviation (cm)	Mean elevation relative to the channel (m)	Mean distance to channel (m)
Upstream	LWAP	17.2 - 71.3	43.7 (+/- 13.9)	2.7 (+/- 1.6)	352.7 (+/- 132.2)
	HWAP	28.3 - 85.3	55.6 (+/- 16.7)	1.1 (+/- 0.6)	359.8 (+/- 61.9)
Midstream	LWAP	42.7 - 121.6	72.9 (+/- 25.1)	3.5 (+/- 0.4)	875.9 (+/- 358.4)
	HWAP	24.2 - 103.8	70.6 (+/- 24.8)	3.8 (+/- 0.3)	387.5 (+/- 98.9)
Downstream	LWAP	20.1 - 90.1	55.1 (+/- 21.2)	5.8 (+/- 0.4)	129.2 (+/- 32.4)
	HWAP	45.5 - 116.2	82.1 (+/- 24.7)	1.9 (+/- 1.1)	92.9 (+/- 16.2)

Table S 1 Summary of trees sampled at the three sites (upstream, midstream, downstream) and in each forest stand (HWAP/LWAP). The distance to the channel was measured with the main channel as reference, without considering the side arms.

Upstream Data Summary

Sampling date	Measure	Number of samplings	mean	sd
2023-04-20	WUE	20	46.754	8.789
2023-05-15	WUE	20	47.988	9.030
2023-05-15	Ψm	40	-1.524	0.319
2023-06-05	WUE	19	50.769	8.162
2023-06-05	Ψm	38	-1.936	0.828
2023-06-26	WUE	19	45.631	9.746
2023-06-26	Ψm	40	-3.246	0.732
2023-07-17	WUE	20	54.988	6.964
2023-07-17	Ψm	40	-3.499	0.705
2023-07-17	Thermal	18	23.611	0.688
2023-08-21	WUE	17	39.662	10.284
2023-08-21	Ψm	40	-3.394	1.229
2023-09-06	WUE	20	38.669	9.006
2023-09-06	Ψm	38	-3.403	0.831
2023-10-04	WUE	20	44.718	9.360
2023-10-04	Ψm	36	-2.919	0.571

Midstream Data Summary

Sampling date	Measure	Number of samplings	mean	sd
2023-04-27	WUE	19	46.332	6.847
2023-04-27	Ψm	39	-1.803	0.327
2023-05-16	WUE	20	49.050	6.575
2023-05-16	Ψm	40	-1.473	0.373
2023-06-06	WUE	20	49.844	7.212
2023-06-06	Ψm	40	-2.048	0.263
2023-06-29	WUE	20	49.960	8.398
2023-06-29	Ψm	40	-3.570	0.984
2023-07-18	WUE	20	42.572	7.124
2023-07-18	Ψm	40	-3.116	0.739
2023-07-18	Thermal	20	28.086	0.639
2023-08-18	WUE	13	45.588	10.090
2023-08-18	Ψm	40	-2.795	0.629
2023-09-07	WUE	20	38.480	8.387
2023-09-07	Ψm	34	-3.422	0.402
2023-10-04	WUE	20	48.715	7.960
2023-10-04	Ψm	36	-3.090	0.762

Downstream Data Summary

Sampling date	Measure	Number of samplings	mean	sd
2023-04-24	WUE	19	46.074	6.334
2023-04-24	Ψm	40	-1.497	0.374
2023-05-15	WUE	20	50.003	7.446
2023-05-15	Ψm	40	-1.953	0.354
2023-06-05	WUE	20	50.686	8.186
2023-06-05	Ψm	38	-2.160	0.600
2023-06-27	Ψm	38	-2.652	0.548
2023-07-12	WUE	20	46.725	6.923
2023-07-12	Ψm	38	-2.893	0.884
2023-07-12	Thermal	20	28.300	0.625
2023-08-17	WUE	19	45.190	4.158
2023-08-17	Ψm	38	-2.847	0.664
2023-09-07	WUE	19	44.931	7.896
2023-09-07	Ψm	34	-3.197	0.771
2023-10-03	WUE	19	45.493	6.179
2023-10-03	Ψm	34	-2.030	0.767

Table S 2 Summary of data collected during the 2023 growing season at the three sites (upstream, midstream, downstream), including sampling date, type of measurement, number of measurements, mean, and standard deviation.